The Plant Cell, Vol. 26: 3449–3467, August 2014, www.plantcell.org

Loss of Ceramide Kinase in *Arabidopsis* Impairs Defenses and Promotes Ceramide Accumulation and Mitochondrial H_2O_2 Bursts[C][W]

Fang-Cheng Bi,[a,1] Zhe Liu,[a,1] Jian-Xin Wu,[a] Hua Liang,[b] Xue-Li Xi,[a] Ce Fang,[a] Tie-Jun Sun,[a] Jian Yin,[a] Guang-Yi Dai,[a] Chan Rong,[a] Jean T. Greenberg,[b] Wei-Wei Su,[a] and Nan Yao[a,2]

[a] State Key Laboratory of Biocontrol, Guangdong Key Laboratory of Plant Resources, School of Life Sciences, Sun Yat-sen University, Guangzhou 510275, P.R. China

[b] Department of Molecular Genetics and Cell Biology, The University of Chicago, Chicago, Illinois 60637

ORCID ID: 0000-0002-2045-5462 (N.Y.)

Arabidopsis thaliana **plants that lack ceramide kinase, encoded by *ACCELERATED CELL DEATH5* (*ACD5*), display spontaneous programmed cell death late in development and accumulate substrates of ACD5. Here, we compared ceramide accumulation kinetics, defense responses, ultrastructural features, and sites of reactive oxygen species (ROS) production in wild-type and *acd5* plants during development and/or *Botrytis cinerea* infection. Quantitative sphingolipid profiling indicated that ceramide accumulation in *acd5* paralleled the appearance of spontaneous cell death, and it was accompanied by autophagy and mitochondrial ROS accumulation. Plants lacking ACD5 differed significantly from the wild type in their responses to *B. cinerea*, showing earlier and higher increases in ceramides, greater disease, smaller cell wall appositions (papillae), reduced callose deposition and apoplastic ROS, and increased mitochondrial ROS. Together, these data show that ceramide kinase greatly affects sphingolipid metabolism and the site of ROS accumulation during development and infection, which likely explains the developmental and infection-related cell death phenotypes. The *acd5* plants also showed an early defect in restricting *B. cinerea* germination and growth, which occurred prior to the onset of cell death. This early defect in *B. cinerea* restriction in *acd5* points to a role for ceramide phosphate and/or the balance of ceramides in mediating early antifungal responses that are independent of cell death.**

INTRODUCTION

In mammals, sphingolipids act as signaling molecules in the regulation of apoptosis, cell proliferation, cell migration, senescence, and inflammation and have been intensively investigated (Hannun and Luberto, 2000; Hannun and Obeid, 2008). Ceramides are key intermediates in sphingolipid biosynthesis and catabolism, acting as precursors in sphingolipid metabolism (Hannun and Obeid, 2008). Endogenous ceramide levels are regulated by integrated metabolic pathways involving specialized enzymes such as ceramide synthases, ceramidases, ceramide kinase, glucosylceramidase, and inositolphosphorylceramidase (Chen et al., 2009).

In plants, a connection between sphingolipids, plant pathogens, and programmed cell death was discovered after treating plants with sphinganine analog mycotoxins that are synthesized by the fungal pathogens *Fusarium moniliforme* and *Alternaria alternata*. These treatments cause programmed cell death with characteristic apoptotic features (Abbas et al., 1994; Wang et al., 1996; Asai et al., 2000). In duckweed (*Lemna pausicostata*), tomato plants (*Solanum lycopersicum*), and tobacco (*Nicotiana tabacum*) cells, treatment with sphinganine analog mycotoxins increases the levels of phytosphingosine and sphinganine, the precursors in de novo synthesis of ceramides (Abbas et al., 1994). Peer et al. (2010) reported that phytosphinganine (t18:0, where t = trihydroxy) exhibits a rapid and transient elevation after inoculation of *Arabidopsis thaliana* with an avirulent strain of the bacterial pathogen *Pseudomonas syringae* pv *tomato*.

Accumulating evidence, mainly from mutant studies, implicates lipid signaling, and ceramides in particular, in regulating plant programmed cell death (Liang et al., 2003; Townley et al., 2005; Shi et al., 2007; Wang et al., 2008; Saucedo-García et al., 2011; Ternes et al., 2011). For example, mutation of the ceramide synthase *LOH1* causes an increase in the level of free trihydroxysphingoid bases and ceramide and glucosylceramide species with a C16 fatty acid and causes spontaneous cell death (Ternes et al., 2011). Elevated ceramide occurs in *myo-inositol 1-phosphate synthase 1* and *inositol phosphorylceramide* synthase mutants of *Arabidopsis* expressing *Resistance to Powdery Mildew 8* (*RPW8*) and is possibly associated with cell death in both mutants (Wang et al., 2008; Donahue et al., 2010). Exogenous ceramides induce calcium-dependent programmed cell death in *Arabidopsis* (Townley et al., 2005). Mitogen-activated protein kinase 6 and reactive oxygen species (ROS) also have been described as transducers that participate in long chain base (LCB)-mediated programmed cell death in plants (Shi et al., 2007; Saucedo-García et al., 2011).

[1] These authors contributed equally to this work.

[2] Address correspondence to yaonan@mail.sysu.edu.cn.

The author responsible for distribution of materials integral to the findings presented in this article in accordance with the policy described in the Instructions for Authors (www.plantcell.org) is: Nan Yao (yaonan@mail.sysu.edu.cn).

[C] Some figures in this article are displayed in color online but in black and white in the print edition.

[W] Online version contains Web-only data.

www.plantcell.org/cgi/doi/10.1105/tpc.114.127050

Ceramide kinase is an enzyme that converts ceramide (Cer) into ceramide 1-phosphate (Cer-1p), a molecule that has a clear signaling function in animal cells (Arana et al., 2010). In *Arabidopsis* plants that have a mutation in *ACCELERATED CELL DEATH5* (*ACD5*), whose product has ceramide kinase activity, plants initially develop normally. However, *acd5* mutants eventually show spontaneous cell death and accumulate ceramide kinase substrates and salicylic acid (SA), a defense signal molecule (Greenberg et al., 2000; Liang et al., 2003). Treatment of *acd5* with an SA agonist can trigger cell death early in development (Greenberg et al., 2000). *ACD5* expression is induced by *P. syringae* infection, and the balance between Cer and Cer-1p modulates cell death in protoplasts (Liang et al., 2003). *acd5* mutants show increased susceptibility to *P. syringae* (Greenberg et al., 2000) and more severe disease symptoms during *Botrytis cinerea* infection (Van Baarlen et al., 2004, 2007).

In this study, we addressed the effects of reduced ceramide kinase levels in *Arabidopsis* during development and infection with *B. cinerea.* We quantified the accumulation of sphingolipids, assessed the timing and spatial location of hydrogen peroxide production, and assayed induction of autophagy and cell wall modifications. Changes in the onset or magnitude of some events in *acd5* plants are correlated with accelerated onset of cell death. However, increased early growth of *B. cinerea* and reduction of some defense responses in plants lacking ceramide kinase occurs prior to cell death. We suggest that there are multiple roles for ceramides in both cell death control and defense against *B. cinerea*.

RESULTS

ACD5 and Ceramide Kinase Activity Localize to Multiple Membrane Compartments

We employed several approaches to identify the subcellular locations of ACD5. Using confocal laser scanning microscopy of protoplasts, ACD5:YFP (yellow fluorescent protein) partially colocalized with markers for the Golgi compartment (Figure 1A, panel 1), endoplasmic reticulum (ER; Figure 1A, panel 2) and plasma membrane (PM; Supplemental Figure 1A). Some ACD5:YFP fluorescence colocalized with CMXRos, a mitochondrial marker (Supplemental Figures 1A to 1C). About 92, 67, 43, and 24% of the ER, PM, Golgi, and mitochondrial markers, respectively, colocalized with ACD5-YFP (Supplemental Figure 1B). Because the ACD5-YFP localization pattern is broad, it seemed possible that the apparent colocalization of signals with mitochondria might be an artifact of the broad YFP signal. To control for this, we rotated the YFP images by 90° and found that the colocalization statistics were reduced from 24 to 14% (Supplemental Figure 1C). This gives added confidence that a pool of ACD5 does colocalize with mitochondria. Additionally, when YFP alone was expressed, it did not colocalize with the mitochondrial marker (Supplemental Figure 1A, left panel).

Immunoelectron microscopy of leaf sections using an ACD5 antibody showed signals in the Golgi, ER, PM, and mitochondria that were significantly higher in wild type versus ACD5RNAi samples (Figures 1B, 1C, and 1F; Supplemental Figure 1D). The ACD5RNAi plants showed a similar visible phenotype to *acd5* mutants (Supplemental Figure 1F) and had greatly reduced protein levels compared with the wild type, as determined by immunoblot analysis (Figure 1D).

Most ceramide kinase activity in *Arabidopsis* is due to ACD5 (Liang et al., 2003). To examine subcellular sites of activity, we used stepwise centrifugation to isolate various cellular compartments and then measured ceramide kinase activity of each compartment. We obtained organelle-rich (P1) and microsome-rich pellets (P2). As verified by immunoblot analysis, the P1 fraction contained more mitochondrial signal (mitochondrial marker, Nad9) and Golgi signal (Golgi α-mannosidase) than plasma membrane signal (PM ATPase) (Supplemental Figure 1G). The P2 fraction was enriched for the plasma membrane signal (Supplemental Figure 1G). We used equal amounts of protein from each of these fractions in activity assays. Ceramide kinase activity was enriched in the P1 and P2 fractions and was the lowest in the S2 fraction (cytosol; Supplemental Figure 1G). We further purified membrane fractions using two-phase partitioning and performed ceramide kinase assays. We separated fractions enriched in PM and intracellular membranes (non-PM). Enzyme assays were performed using equal amounts of protein from total extract (total), cleared total lysate (C), cytosol (S2), total membrane fraction (P2), PM fraction (PM), and intracellular membrane fractions (non-PM) (Supplemental Figure 1H). PM and intracellular membrane fractions showed higher activity compared with total extracts, indicating that ceramide kinase was both localized to and enriched in these membranes. The fractions were also probed with antibody markers for Golgi (α-mannosidase), plasma membrane (ATPase), and ER (ACA2) to assess the purity of the fractions (Supplemental Figure 1H).

Taken together, ACD5 protein and enzyme activity mainly exist in ER and Golgi as reported in mammalian cells and also partially localizes plasma membrane and mitochondria.

Mitochondrial ROS Is Associated with Ceramide-Induced Cell Death

Because some ACD5 localized to mitochondria, we explored the possibility that mitochondrion-related events occurred during ceramide accumulation. We previously found that C2 ceramide induces mitochondrial membrane potential loss and cytochrome c release (Yao et al., 2004). Here, we focused on the accumulation of ROS in mitochondria because this can be causal to cell death (Yao et al., 2002; Zhou et al., 2011; Pattanayak et al., 2012). To detect sites of H_2O_2 accumulation, we performed histochemical staining using cerium chloride ($CeCl_3$), which reacts with H_2O_2 to produce electron dense precipitates of cerium perhydroxide that can be visualized using electron microscopy (Yao et al., 2002). Under our growth conditions, the cell death phenotype of *acd5* began to appear ~30 d after planting. In 20- and 40-d-old wild-type leaves, no H_2O_2 was detected in cells (Figure 2A). However, cerium deposits were frequently observed in 40-d-old *acd5* rosette leaves. H_2O_2 accumulated on outer and inner membranes of mitochondria (Figure 2B), in autophagosome-like structures (Figure 2C), and in the cytosol (Figure 2D) of cells near a dying cell in *acd5*. Large lipid drops were also observed in 40-d-old *acd5* plants (Figures 2B and 2D).

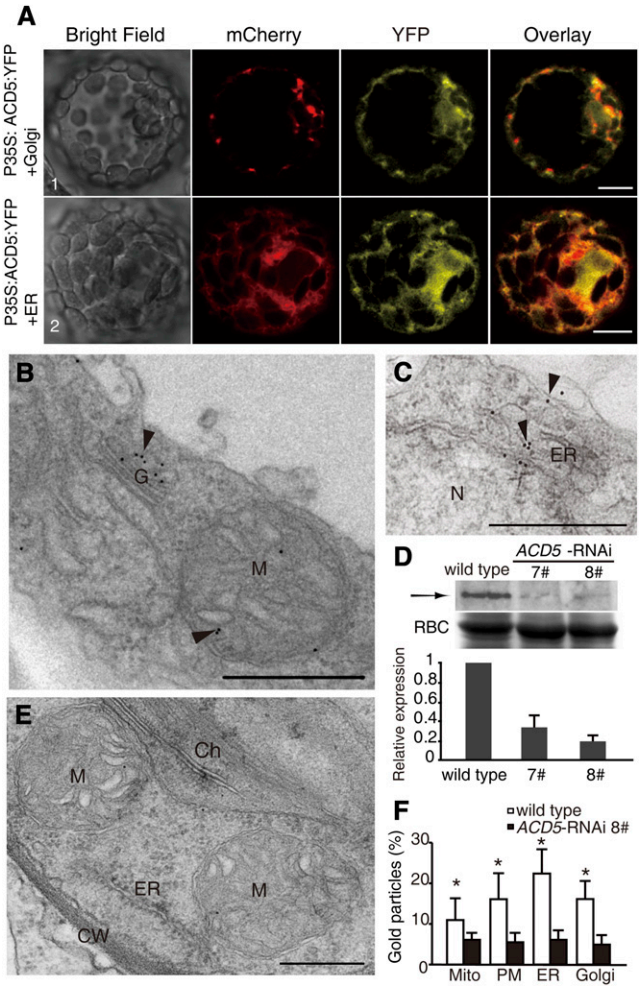

Figure 1. Subcellular Distribution of *Arabidopsis* Ceramide Kinase.

(A) Subcellular localization of ACD5/ceramide kinase. The coding region of ACD5 was fused with the YFP at the C terminus, and then ACD5:YFP was coexpressed with a Golgi mCherry marker (ABRC stock number, CD3-968, row 1 panels) or an ER mCherry marker (TAIR, CD3-960, row 2 panels) by transient expression in *Arabidopsis* protoplasts. Protoplasts were examined by confocal microscopy 16 to 22 h after incubation. This experiment was repeated at least three times with similar results, and more than 20 protoplasts were analyzed at each time point (one protoplast is shown in each image). Bars = 10 μm.

(B) and **(C)** Immunolocalization of ACD5 in wild-type plants. Arrowheads indicate the particles of immunogold-labeled ACD5. G, Golgi, M, mitochondrion; N, nucleus. Bar = 500 nm.

(D) Immunoblot analysis of ACD5 in *ACD5*-RNAi (lines 7 and 8) and wild-type plants. Equal quantities of proteins extracted from 14-d-old plants were detected with an ACD5 antibody (upper panel). Coomassie blue staining of Rubisco (RBC) large subunit bands was for a loading control (middle panel). Protein levels were quantified as described in Methods (lower graph). Values are mean ACD5 levels relative to the wild-type control (set at 1). Error bars represent ±SD for three biological replicates.

(E) Immunolocalization of ACD5 in *ACD5*-RNAi plants (line 8). Note that few particles of immunogold-labeled ACD5 were observed. Ch, chloroplast; M, mitochondrion. Bar = 500 nm.

(F) Statistical analysis of ACD5 localization by immunoelectron microscopy in wild-type and *ACD5*-RNAi plants. Twenty mesophyll cells in each experiment were observed, and at least 30 photos were used for counting. Values are means ± SD. At least three independent experiments were done with similar results. Asterisks indicate significant differences between wild-type and *ACD5*-RNAi plants at $P < 0.05$ using Student's *t* test. The percentage of gold particles means percentage of the particle numbers of each organelle in the total amount of particles.

Treatment of protoplasts isolated from 18-d-old wild-type plants with 30 μM C2 ceramide produced ROS within 1 h. Interestingly, as detected by CM-H_2DCFDA staining, the ROS colocalized with mitochondria labeled by CMXRos (Figure 2E). When we coincubated protoplasts with ceramide and cyclosporin A, which blocks mitochondrial membrane potential loss during treatments with protophoryin IX (Yao et al., 2004), the ROS was undetectable (Supplemental Figure 2). Coincubation of cells with ceramide and C2 ceramide1-phosphate, the protein kinase inhibitor K252a, or the antioxidant *N*-acetylcysteine (NAC), respectively, similarly reduced ROS accumulation (Supplemental Figure 2). NAC partially and K252a or the protein synthesis inhibitor cycloheximide completely prevented C2-induced cell death (Figures 2F and 2G). Thus, in *acd5* cells late in development and in wild-type protoplasts treated with exogenous ceramides, a major site of ROS production was in mitochondria. Importantly, this production also required protein kinase activity and new protein synthesis. These experiments show that mitochondrial ROS produced when ceramides accumulate is correlated with cell death.

Autophagy Is Activated in *acd5* Late in Rosette Development

Autophagy in plants is a mechanism to recycle nutrients and breakdown cellular components such as organelles that may be damaged (Hayward and Dinesh-Kumar, 2011). Since ultrastructural analysis of leaves from 40-d-old *acd5* plants showed autophagasome-like structures (Figure 2C), we further tested the status of the autophagy pathway. When compared with wild-type plants, the transcripts of all six tested autophagy-related genes showed significant differences in expression in *acd5* plants on days 30 and 40 (Figure 3A). To quantify the possible presence of autophagosomes, we generated wild-type and *acd5* plants that express a *GFP-ATG8e* fusion. Upon concanamycin A treatment (to block degradation of autophagosomes in vacuoles; Yoshimoto et al., 2004), many punctate structures representing the autophagosomes in 40-d-old *acd5* leaves were observed using confocal microscopy. By contrast, fewer such structures were observed in wild-type leaves (Figures 3B to 3D). In 20-d-old leaves (before cell death occurred in *acd5*), there was no difference in the number of autophagosomes accumulated in wild-type and *acd5* leaves (Figures 3B and 3D). These data suggest that the autophagy program was activated in *acd5* late in development.

Ceramides Accumulate Late during *acd5* Rosette Development

Arabidopsis acd5 mutants accumulate more ceramide kinase substrates than in wild-type plants late in development (Liang et al., 2003). To determine the chemical nature of potential

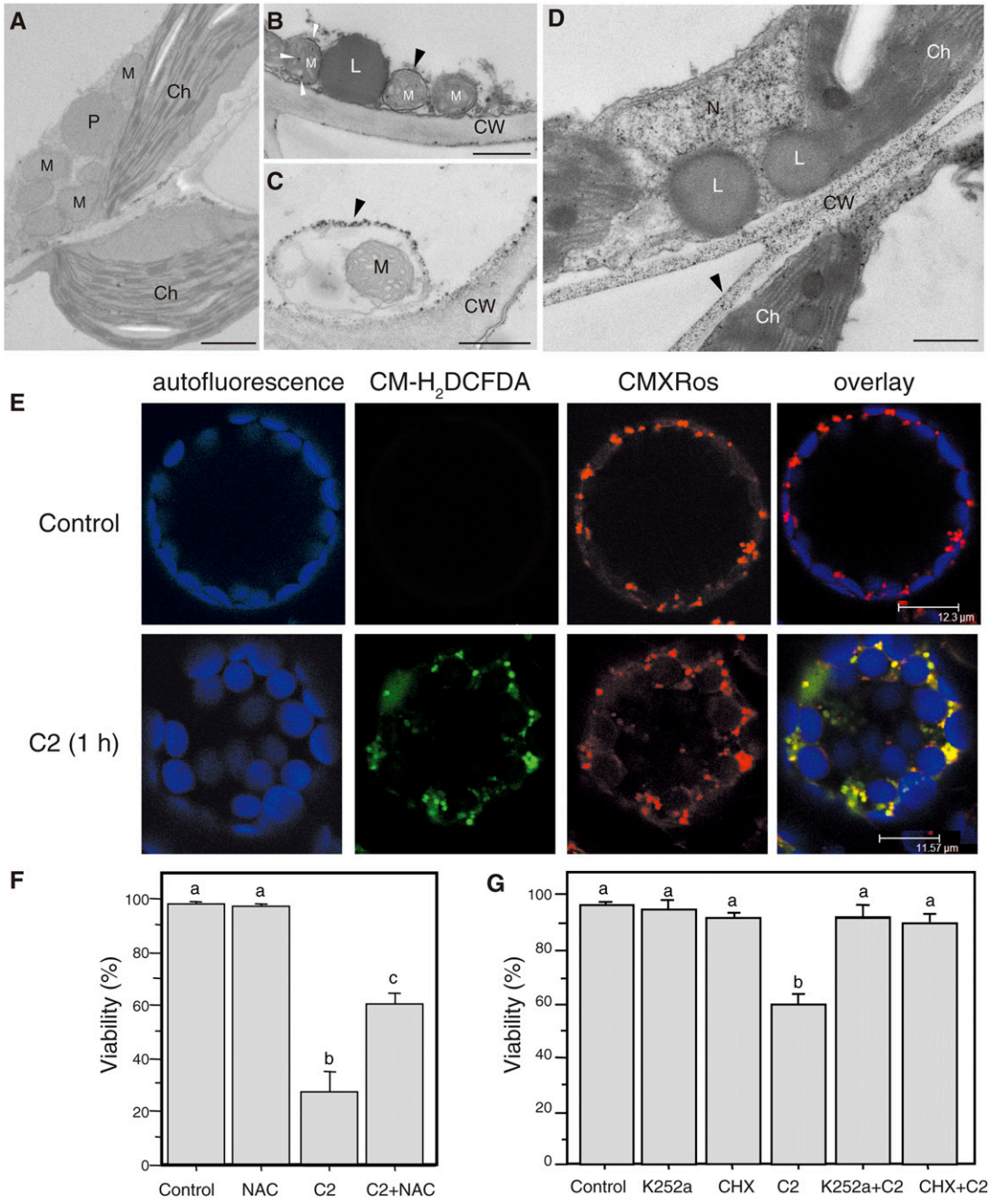

Figure 2. ROS Localization in Late Development of *acd5* Plants and in Ceramide-Treated Protoplasts.

(A) to **(D)** Forty-day-old wild-type leaves and *acd5* mutant leaves with spontaneous cell death were pretreated with cerium chloride to visualize H_2O_2 production as described in Methods and were observed by electron microscopy without staining. At least three different leaf samples of both wild-type and *acd5* plants were cut in each experiment. Images represent typical observations in two independent experiments. Bars = 500 nm.

(A) Wild-type mesophyll cells. Note that all organelles are cerium-free.

(B) to **(D)** *acd5* mutant mesophyll cells. Note electron-dense cerium deposits (arrowheads), indicative of the presence of H_2O_2 in mitochondrial outer and inner membranes **(B)**, autophagosome-like structure membrane **(C)**, and cell wall **(D)**. Ch, Chloroplast; CW, cell wall; L, lipid drop; M, mitochondrion; N, nucleus; P, peroxisome.

(E) ROS production induced by C2-ceramide treatment of protoplasts. Protoplasts were isolated from 18-d-old wild-type leaves, treated with 0 (Control) or 30 μM C2-ceramide (C2) for 1 h under light, and then double stained with CM-H_2DCFDA (to detect ROS) and CMXRos (mitochondrial marker). Chloroplast autofluorescence was excited at 488 nm and detected at 738 to 793 nm (shown in blue). Images were taken by confocal laser scanning

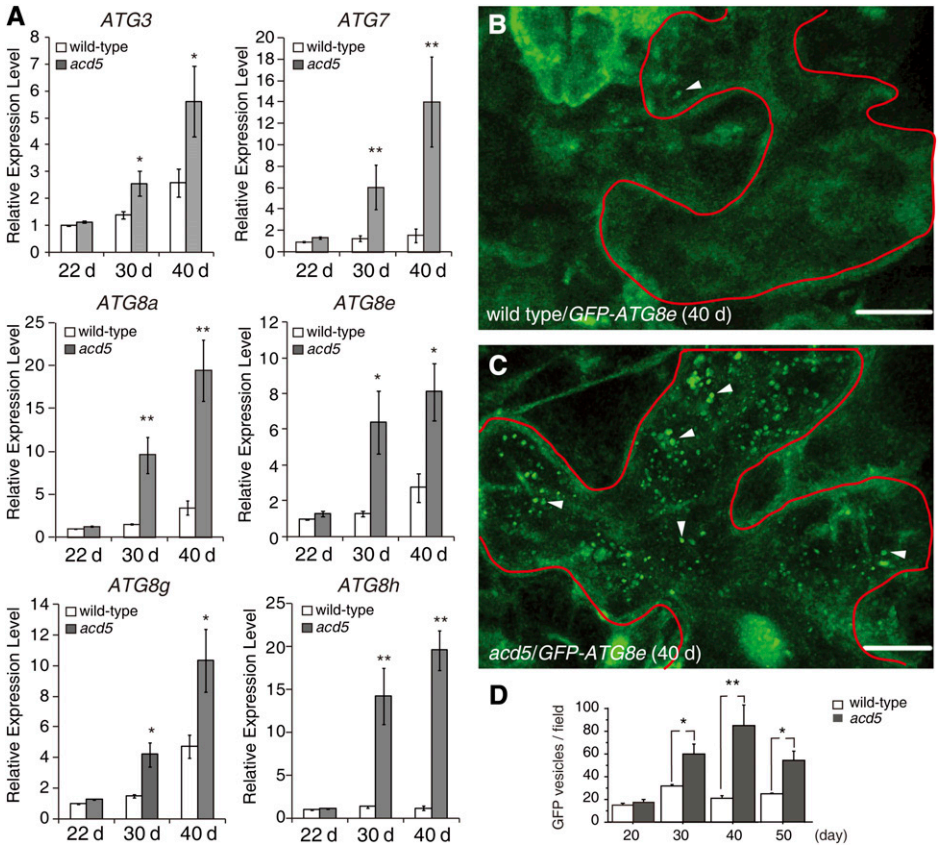

Figure 3. Induction of Autophagy in *acd5* Plants.

(A) Expression level of autophagy-associated genes. The genes analyzed were *ATG3*, *ATG7*, *ATG8a*, *ATG8e*, *ATG8g*, and *ATG8 h*. Total RNA was extracted at the indicated days for quantitative RT-PCR analysis of gene expression. *ACT2* encoding actin was used as an internal control. Gene expression values are relative to average wild-type levels of 22-d-old plants (set as 1). This experiment was repeated three times using independent samples. Values are means ± SD from three biological replicates. Significant differences were determined by Student's *t* test (*P < 0.05 and **P < 0.01). The primers used for these analyses are provided in Supplemental Table 1.

(B) and **(C)** Detection autophagic vesicles inside the vacuole using GFP-ATG8e fusion. Different developmental stages of wild-type and *acd5* plant leaves expressing a GFP-ATG8e fusion were infiltrated with 1 μM concanamycin A for 1 d. The detached leaves were visualized by confocal microscopy. Note abundant autophagosomes (arrowhead) in 40-d-old *acd5* leaves. Bars = 10 μm.

(D) Statistical analysis of number of GFP vesicles as shown in **(B)** and **(C)** in different developmental stages of wild-type and *acd5* leaves. Twelve detached wild-type or *acd5* leaves were observed in each developmental stage. Values are means ± SE. Significant differences were determined by Student's *t* test (*P < 0.05 and **P < 0.01) from three biological repeats.

substrates and determine how the sphingolipid pathway was perturbed in *acd5*, we compared the sphingolipid content of *acd5* and wild-type rosettes at different developmental stages. We used HPLC electrospray tandem mass spectrometry to quantify sphingolipids (Markham and Jaworski, 2007). Comparative analysis of the sphingolipid profiles indicated that the total amounts of ceramides in *acd5* plants showed progressive increases over time and were higher than those in the wild-type plants after day 22 (Figures 4A and 4D; Supplemental Table 2). In 40-d-old plants, ceramides were ~4-fold higher in *acd5* than in the wild type (Figure 4A).

Figure 2. (continued).

microscopy. At least 300 protoplasts were observed, and over 80% of protoplasts showed ROS signal. See Supplemental Figure 2 for the effects of different treatments on ROS production. This experiment was repeated three times with similar results.

(F) and **(G)** Percentage of survival of wild-type protoplasts after ceramide treatment and coincubation of a ROS scavenger or inhibitors of protein kinase or protein synthesis, respectively. Protoplasts were isolated from 19-d-old wild-type leaves and then treated with chemical reagents under light. Cell viability was determined by fluorescein diacetate staining. Letters indicate statistically different values using a Student-Newman-Keuls *t* test, P < 0.05. For each treatment, at least 800 protoplasts were counted. Values are means ± SD from two independent experiments.

(F) Effects of 5 μg/mL NAC on 30 μM C2 ceramide-induced cell death at 24 h.

(G) Effects of 100 nM K252a and 10 μM cycloheximide (CHX) on 30 μM C2 ceramide-induced cell death at 5 h.

In the case of hydroxyceramides, their accumulation was modestly elevated relative to the wild type in *acd5* even in 17-d-old plants and increased ~2- to 6-fold relative to the wild type in 40-d-old plants (Figures 4A and 4B; Supplemental Table 3). Moreover, ceramide-containing long-chain fatty acids (C16) exhibited a more dramatic increase than ceramide-containing very-long-chain fatty acids (C24 and C26) (Figures 4C and 4D). No significant changes were observed in levels of the other two sphingolipids, LCBs and glucosylceramides, at all stages tested (Figures 4A; Supplemental Figure 3). Most ceramide species in *acd5* gradually increased starting on day 22, and some species showed more dramatic increases when spontaneous cell death began to appear and reached higher levels late in development (Figure 4D; Supplemental Table 2). The pattern of increase was comparable between hydroxyceramide species containing long-chain fatty acids and hydroxyceramide species containing very long chain fatty acids (Figure 4C; Supplemental Table 3). Thus, accumulation of ceramides, especially long-chain ceramides, was correlated with spontaneous cell death in *acd5* plants.

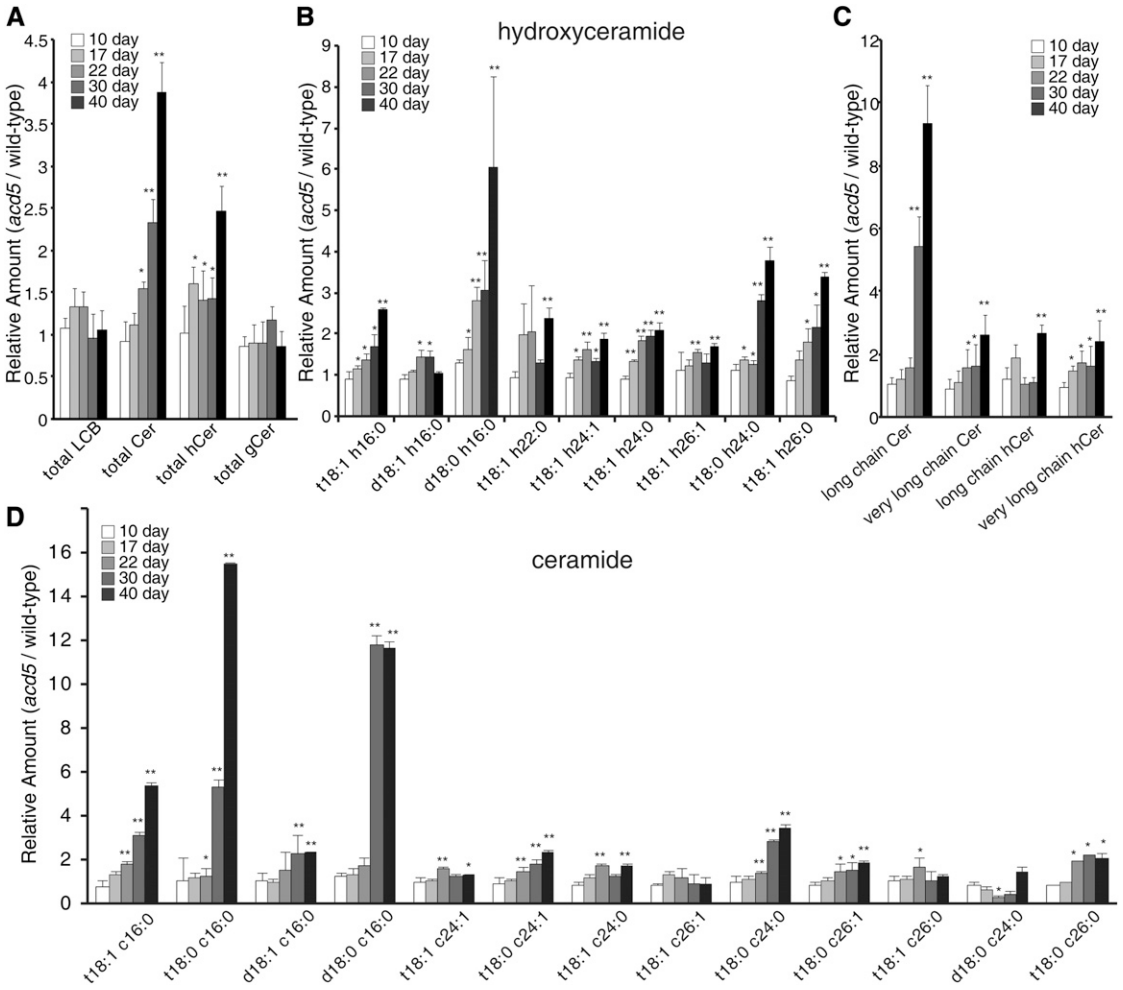

Figure 4. Sphingolipid Content Alteration during *acd5* Development.

Sphingolipids were extracted from rosettes of soil-growth *Arabidopsis* leaves at different developmental stages. The amounts of free LCBs, main glucosylceramides, main hydroxyceramides, and main ceramides in wild-type and *acd5* leaves were quantified after extraction, separation, and identification by HPLC coupled with electrospray ionization tandem mass spectrometry as described in Methods. Values indicate the absolute level of sphingolipids in *acd5* relative to the level found in the wild type (set as 1) ±SD from four independent experiments. Significant differences between *acd5* and the wild type at each time point were determined by Student's *t* test (*P < 0.05 and **P < 0.01) (see Supplemental Tables 2 and 3 for the absolute values).

(A) Measurement of sphingolipids from *acd5* relative to wild-type leaves at different times included total LCBs, glucosylceramides (gCer), hydroxyceramides (hCer), and ceramides (Cer).

(B) Measurement of hydroxyceramide species in *acd5* relative to wild-type leaves at different times.

(C) Measurement of total long acyl chain length (C16, C18) and very long acyl chain length (>C18) ceramides or hydroxyceramides at different times in *acd5* relative to the wild type.

(D) Measurement of various ceramide species in *acd5* relative to wild-type leaves at different times.

Ceramide Accumulation Is a Key Factor in the Timing of the *acd5* Cell Death Phenotype

Endogenous ceramides are generated either from de novo synthesis or from the catabolism of sphingolipids (Chen et al., 2009). To determine whether one of these mechanisms is prevalent, we measured transcript levels of genes related to ceramide accumulation by quantitative RT-PCR. The *acd5* plants had higher transcript levels of three ceramide synthase genes (*LOH1*, *LOH2*, and *LOH3*) and lower expression of three putative ceramidase genes (*At1g07380*, *At2g38010*, and *At5g58980*), consistent with their protein products contributing to accumulation of ceramides late in development of *acd5*, compared with wild-type plants (Figure 5A). Differences in transcript levels of other tested genes, such as inositolphosphoceramide synthetase (*IPCS*), inositolphosphorylceramidases (*IPCD*), and homologs of bile acid β-glucosidase (glucosylceramidase [*GCD*]), were modest (2-fold or less; Supplemental Figure 4). We also found that *ACD5* expression levels increased during plant development (Supplemental Figure 5A).

We used a genetic approach to further investigate the relationship between ceramide accumulation and cell death in *acd5* mutants. LOH1 and LOH3 are responsible for biosynthesis of very-long-chain (C20-C28) ceramide species, and *loh1* knockout plants show spontaneous cell death under short-day conditions and *loh3* has no visible phenotype (Ternes et al., 2011). Twenty-five-day-old double mutant *acd5 loh3* plants showed severe cell death and a reduced growth habit, whereas each single mutant had a visible phenotype similar to the wild type (Figure 5B). *LOH* gene expression levels in *acd5* and wild-type plants were the same in 22-d-old plants (Figure 5A). However, at the same development stage, *LOH2* showed more than 3-fold higher expression in *acd5 loh3* than wild-type plants (Figure 5C). Strikingly, there was a dramatic increase in ceramide accumulation, especially C16 ceramides in *acd5 loh3* plants compared with the wild type and each single mutant (Figures 5D and 5E; Supplemental Tables 4 and 5). Similar phenotypes were also observed in *acd5 loh2* double mutants (Supplemental Figure 6A) and ceramide profile analysis revealed a dramatic increase in very-long-chain ceramides in *acd5 loh2* plants compared with the wild type and each single mutant (Supplemental Figure 6B and Supplemental Table 6). These results showed that not only long-chain (C16, C18), but also very-long-chain (>C18) ceramides contribute to cell death. Thus, the increased ceramide synthase levels in *acd5* promote ceramide accumulation and leads to the accelerated cell death phenotype.

B. cinerea Shows Increased Early Growth in *acd5* Plants

acd5 mutants show increased susceptibility to *P. syringae* (Greenberg et al., 2000) and display increased cell death during *B. cinerea* infections (Van Baarlen et al., 2004, 2007). We confirmed that *acd5* shows more severe symptoms than the wild type after infection with *B. cinerea* (Supplemental Figures 7A and 7B). To determine whether increased symptoms after *B. cinerea* infection were due to greater pathogen growth, we assessed fungal germination and growth in inoculated plants by trypan blue staining. In comparison with wild-type plants, on *acd5* plants, conidial germination rates and hyphae lengths (Figures 6A and 6B) of *B. cinerea* were higher and longer, respectively, at all time points tested. At 18 h postinoculation (hpi), the lengths of hyphae were ~3 times higher on the *acd5* mutants than on wild-type plants (Figure 6B; Supplemental Figure 7C). Thus, wild-type plants effectively restricted fungal growth, while *acd5* plants did not. Trypan blue staining also allowed an assessment of plant cell death, which was not associated with the early increase in *B. cinerea* growth (note the lack of stained plant cells in Supplemental Figure 7C). Additionally, no cell death lesions appeared before infection in *acd5* plants, indicating that the susceptibility of *acd5* to *B. cinerea* was not due to the presence of spontaneous cell death lesions before inoculation. In 2% glucose mock-treated leaves, no cell death was observed in both wild-type and *acd5* plants (Supplemental Figure 7D, lower panels). However, *B. cinerea*-inoculated leaves showed more cell death in *acd5* plants than the wild type by 36 hpi (Supplemental Figure 7D, upper panels). Taken together, the *acd5* mutation resulted in increased susceptibility to *B. cinerea*, as determined by increased growth of the pathogen in host tissue prior to induction of cell death.

B. cinerea-Induced Defenses Are Impaired in *acd5* Plants

Increased growth of *B. cinerea* in *acd5* plants might be caused by impaired defense-related responses in the host. Thus, we examined several defense responses. First, we assayed the levels of ROS using 3,3′-diaminobenzidine (DAB) staining within the first 3 d after inoculation with *B. cinerea*. Inoculated plants generated brown precipitate indicative of ROS production, and this precipitate was completely absent in 2% glucose inoculated wild-type and *acd5* plants (Figure 6C). In wild-type plants, as early as 18 hpi, obvious DAB signals were observed and increased to give similar levels at 36 and 72 hpi (Figure 6C). Relative to the wild type, *acd5* had less DAB staining at earlier times (18 and 36 h) but more DAB staining later (72 h). Thus, the kinetics of ROS accumulation differed in wild-type plants relative to *acd5* plants after *B. cinerea* infection.

To precisely determine the sites of ROS accumulation, production of H_2O_2 after infection was examined with $CeCl_3$ to allow visualization of electron dense precipitates of cerium perhydroxide (Yao et al., 2002). Cerium perhydroxide precipitates were first observed on cell walls at early infection times in both *acd5* and wild-type plants (Figures 6D and 6E). However, wild-type plants exhibited more intense staining of $CeCl_3$ on cell walls (over 10 times higher) than *acd5* mutants at the early infection stage (Figures 6G and 6H). In *acd5*, cerium deposits appeared on mitochondria at 24 hpi (Figure 6F), which was 12 h earlier than their appearance in wild-type plants (Figure 6J). We observed more than 12 different sections from four different leaf blocks and found that no H_2O_2 accumulated in mitochondria before 24 hpi in the wild type, whereas two out of four *acd5* leaf blocks (at least 16 sections) showed mitochondrion-derived H_2O_2 accumulation at 24 hpi. At 48 hpi, a mitochondrial oxidative burst was observed more frequently at the cell adjacent to dead cells in *acd5* (Figure 6I) and the dying cell in the wild type (Figure 6K). This observation may explain the earlier and/or more extensive appearance of dead plant cells in *B. cinerea* infected *acd5* leaves (Supplemental Figure 7), since mitochondrial ROS

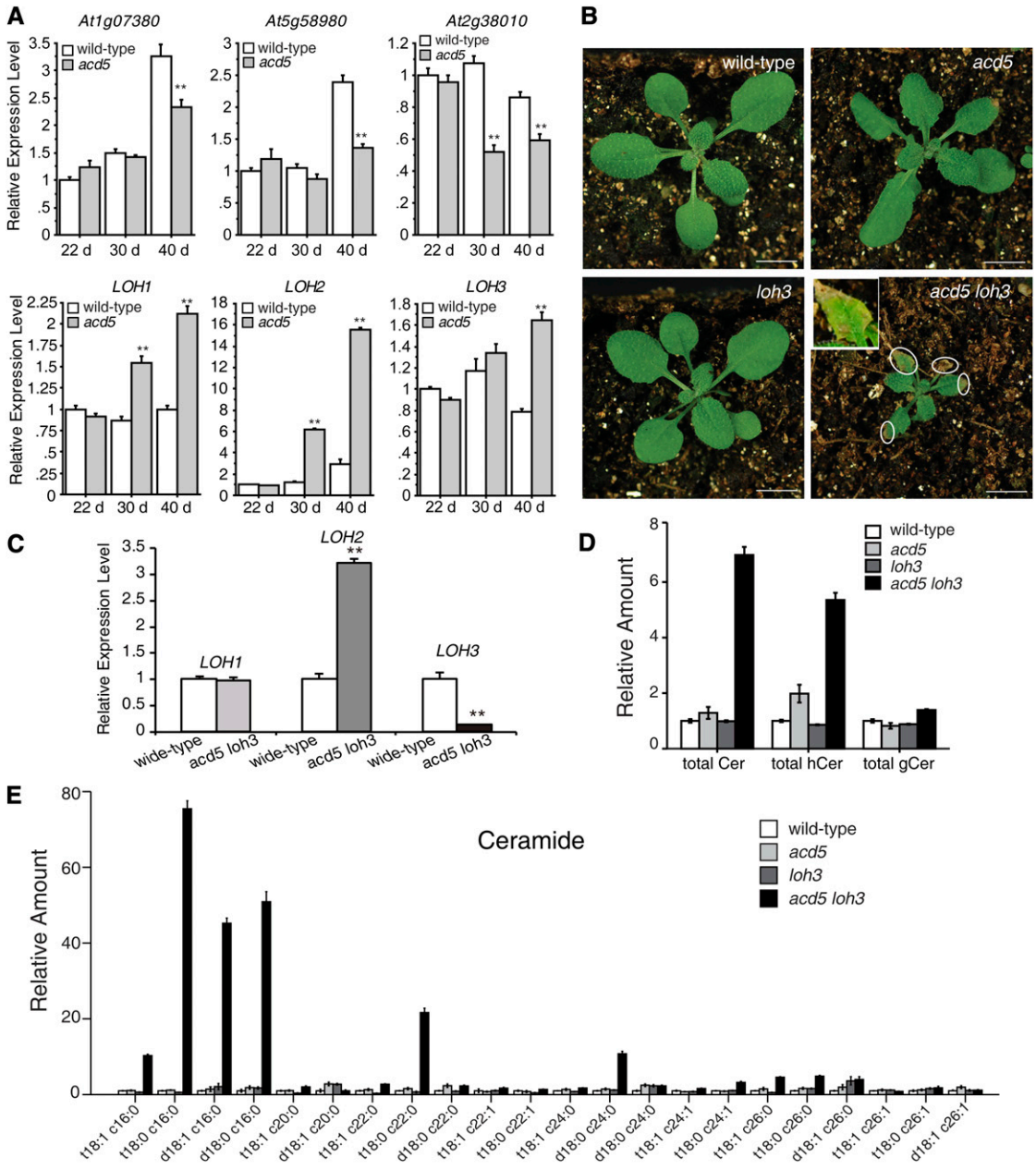

Figure 5. Expression of Sphingolipid Metabolism Related Genes and Sphingolipid Content Alteration in *acd5* and *acd5 loh3* Double Mutants.

(A) Expression of sphingolipid metabolism related genes in *acd5* and wild-type plants. The genes chosen were three ceramide synthetase genes *LOH1* (At3G25540), *LOH2* (At3G19260), and *LOH3* (At1G13580) and three candidate ceramidase genes: At1g07380, At5g58980, and At2g38010. Total RNA was extracted at the indicated time points for quantitative RT-PCR. *ACT2* was used as an internal control. Gene expression values are presented relative to average wild-type levels of 22-d-old plants (set as 1). This experiment was repeated three times using independent samples. Values are means ± SD from triplicate biological repeats. Significant differences were determined by Student's *t* test (**P < 0.01). The primers used for these analyses are provided in Supplemental Table 1.

(B) The *acd5 loh3* double mutant phenotype. Photos are of 25-d-old plants. The white circles and the square indicate cell death lesions in *acd5 loh3*. Bar = 0.5 cm.

(C) The transcript levels of ceramide synthetase genes in *acd5 loh3* mutants. Total RNA was extracted from 22-d-old plants. *ACT2* was used as an internal control. Gene expression values are presented relative to average wild-type levels (set as 1). This experiment was repeated two times using independent samples. Values are means ± SD from two biological repeats. Significant differences were determined by Student's *t* test (**P < 0.01).

(D) and **(E)** Sphingolipid levels in *acd5 loh3* mutants. The accumulation values indicate the absolute level of sphingolipids in 25-d-old *acd5*, *loh3*, and *acd5 loh3* relative to that found in the wild type (set as 1).

(D) The amount of total ceramides (Cer), hydroxyceramides (hCer), and glucosylceramides (gCer).

(E) Various ceramide species. Values represent means ± SD from two independent experiments (see Supplemental Tables 4 and 5 for the absolute values).

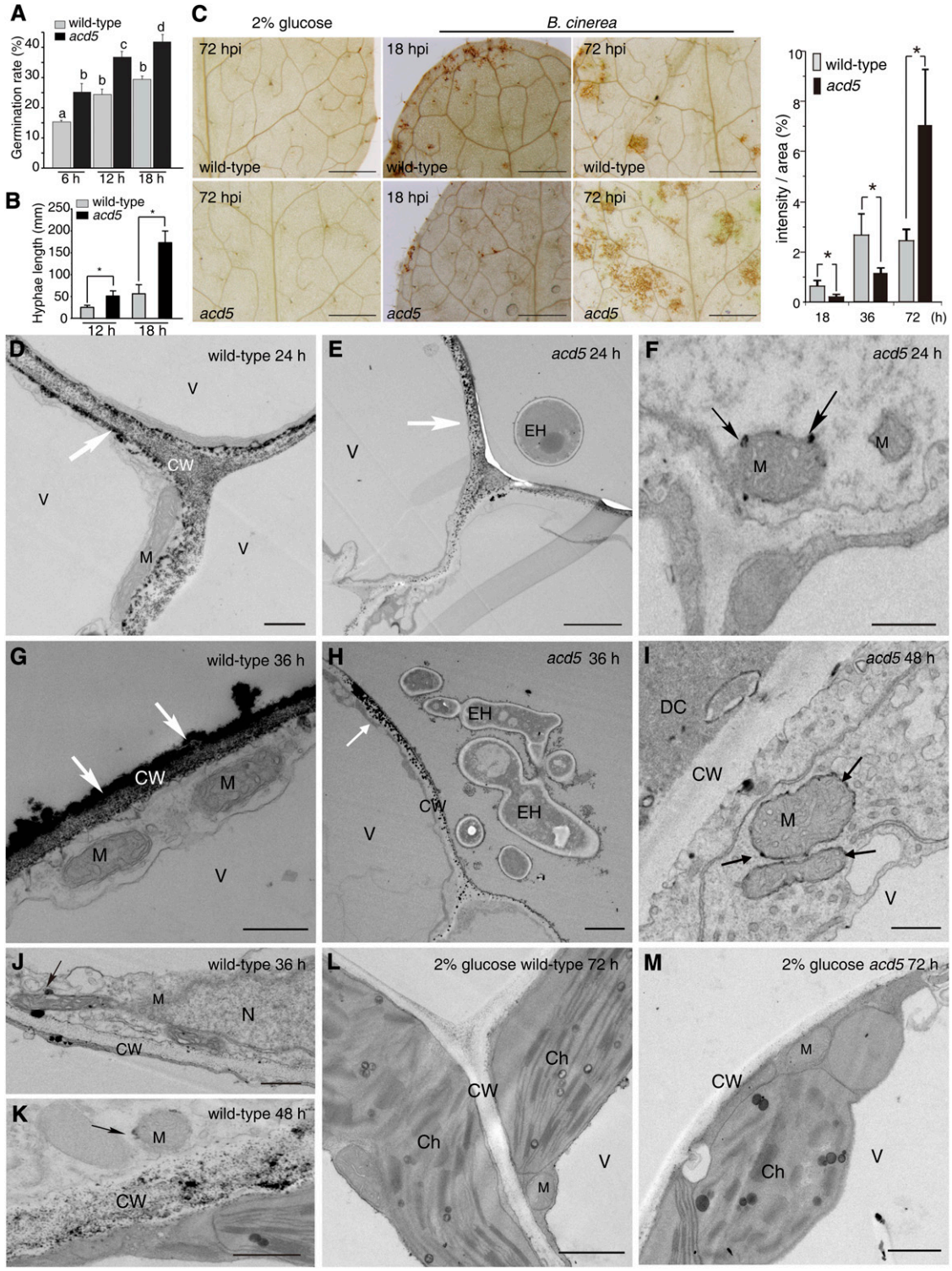

Figure 6. ROS Production in Wild-Type and *acd5* Leaves after *B. cinerea* Infection.

(A) Percentage of germination of *B. cinerea* at the indicated times after spraying conidia on wild-type and *acd5* leaves. Conidial germination was visualized using trypan blue staining and counted by microscopy. This experiment was repeated more than three times with similar results, and more than 18 leaves in the wild type or *acd5* were counted at each time point. Letters indicate significantly different values using Fisher's protected least significant difference, a post-hoc multiple *t* test ($P < 0.01$). Error bars indicate SD from three independent tests.

accumulation is often associated with cell death (Yao et al., 2002; Zhou et al., 2011; Pattanayak et al., 2012). In the mock-inoculated leaves, no electron-dense deposits were observed in wild-type and *acd5* mutant plants at any time point tested (Figures 6L and 6M).

We also assayed cell wall-based defenses at both light and electron microscopy levels after inoculation with *B. cinerea* and/or chitin, a pathogen-associated molecular pattern derived from fungi (de Jonge et al., 2010). No detectable callose deposits were found in mock-inoculated wild-type or *acd5* plants (Supplemental Figure 8A). In response to *B. cinerea* infection, wild-type plants showed more callose deposits than the *acd5* plants (Figure 7A; Supplemental Figure 8A). Similar responses were found using chitin. Almost no callose deposits in *acd5* were observed after 12-h chitin treatments, whereas scattered callose deposits were found in wild-type plants at this time and dramatically increased at 24 h (Supplemental Figure 8B; Figure 7C). At 72 h after *B. cinerea* infection, more cell death was observed in *acd5* mutants than wild-type plants (Figure 7B). Also at 72 h, large cell wall appositions (papillae) with ROS accumulation (recognized by cerium deposits) were frequently observed in wild-type plants (Figure 7D). However, cell wall appositions were much smaller, lacked cerium deposits, and were only rarely observed in *acd5* plants (Figure 7E).

Expression of several defense-related genes was also compromised in *acd5* plants after infection. Peroxidases and chitinases act in cell wall related defenses and resistance to a wide range of pathogens (Daudi et al., 2012). *B. cinerea* infection activated expression of peroxidase *PRX33* and *PRX34* genes in the wild type, but not in *acd5* mutants; similar results were also obtained for expression of a chitinase family gene (Figure 7F). *PR1* induction was impaired in the *acd5* mutants, in contrast to its strong early induction in wild-type plants (Figure 7F). Previous reports established that resistance to necrotrophic fungal pathogens in plants is strongly dependent upon the production of camalexin, an indole-type phytoalexin (Thomma et al., 1999). Therefore, we examined the expression of *PAD3* and *CYP71A13*, key genes in camalexin synthesis. After infection, lower accumulation of both gene transcripts was observed in *acd5* plants compared with wild-type plants (Figure 7F).

In summary, the loss of ceramide kinase impairs the timely induction of defenses at the cell periphery and the induction of defense-related gene expression, while causing increased mitochondrial ROS and cell death. One or more of these changes likely facilitates *B. cinerea* germination, growth, and propagation.

B. cinerea Induces Greater Ceramide Accumulation in *acd5* Than in the Wild Type

The effect of *acd5* on *B. cinerea*-induced symptoms suggested that sphingolipid content might be altered during infection. In wild-type plants, the total amounts of ceramides and hydroxyceramides showed large increases especially on days 3 and 4 after infection relative to glucose-inoculated control (Figure 8A). Except hydroxyceramides containing d18:1, the hydroxyceramides containing t18:0, t18:1, and d18:0 also increased in wild-type plants, usually showing large increases (3- to 14-fold) starting on day 3 or 4 after *B. cinerea* infection (Figure 8B). Moreover, most tested ceramides and hydroxyceramides exhibited a similar accumulation pattern, showing increases starting on day 2 or 3, peaking on day 3 or 4 and then decreasing on the 5th day (Figures 8C to 8E; Supplemental Table 7). In addition, the relative accumulation of hydroxyceramides was much higher compared with that of ceramides, and this was reminiscent of the sphingolipid analysis of *acd5* plants at various developmental ages. These data indicated that accumulation of ceramides was associated with the plant response to *B. cinerea* infection. Consistent with ceramide accumulation, *ACD5* expression was induced by day 3 after infection in the wild type (Supplemental Figure 5B).

In *acd5* plants, total ceramides increased to a greater extent than in the wild type, especially by day 5 after inoculation, when an ~3-fold increase was detected (Figure 8F). Most individual ceramide species showed levels comparable to that observed in wild-type plants after infection (Figures 8H and 8I). However, the total hydroxyceramide content increased 3-fold in the first day,

Figure 6. (continued).

(B) Lengths of hyphae on wild-type and *acd5* leaves after *B. cinerea* infection. The lengths of hyphae were measured with Leica LAS software. A total of ~30 to 50 hyphae per leaf and a total of six leaves in each genotype were measured in each experiment. Asterisks indicate a significant difference from the wild type using Student's *t* test (*$P < 0.01$). This experiment was repeated three times with similar results and more than 150 hypha were measured each time. Error bars indicate SD from three independent tests.

(C) Accumulation of ROS in wild-type and *acd5* leaves at indicated times after 2% glucose (control) or *B. cinerea* inoculation. Leaves were stained with DAB as described in Methods. The brown precipitate indicated DAB polymerization at the site of ROS production. The right panel shows quantification of DAB staining as the percentage and intensity of leaf area stained from 18 leaves per genotype measured using ImageJ software as described in Methods. Error bars indicate SD from three independent experiments. Asterisks indicate a significant difference from the wild type using Student's *t* test ($P < 0.05$). Bars = 1 mm.

(D) to **(M)** H_2O_2 localization observed by electron microscopy using cerium chloride staining after inoculation with 2% glucose or *B. cinerea*. The left panels are wild-type leaves inoculated with *B. cinerea* for 24 h **(D)**, 36 h (**[G]** and **[J]**), and 48 h **(K)**. Note that heavy cerium deposits (white arrows) were observed in the cell wall at 24 to 36 h (**[D]** and **[G]**), but not in mitochondria. The middle and right panels are *acd5* leaves inoculated with *B. cinerea* for 24 h (**[E]** and **[F]**), 36 h **(H)**, and 48 h **(I)**. Note the presence of cerium deposits in both the cell wall (**[E]**, white arrow) and the outer membrane of mitochondria (**[F]**, black arrows) in 24 h *acd5* samples. Mock-treated wild-type **(L)** and *acd5* **(M)** leaves at 72 h stained with cerium chloride. Note the lack of H_2O_2 from the beginning of control treatment up to 72 h (**[L]** and **[M]**). Arrows indicate depositions of cerium. Ch, chloroplast; CW, cell wall; DC, dead cell; EH, extracellular hyphae; M, mitochondrion; N, nucleus; V, vacuole.

Bars = 2 μm in **(E)** and **(H)**, 1 μm in **(D)**, **(J)**, **(L)**, and **(M)**, and 0.5 μm in **(F)**, **(G)**, **(I)**, and **(K)**.

[See online article for color version of this figure.]

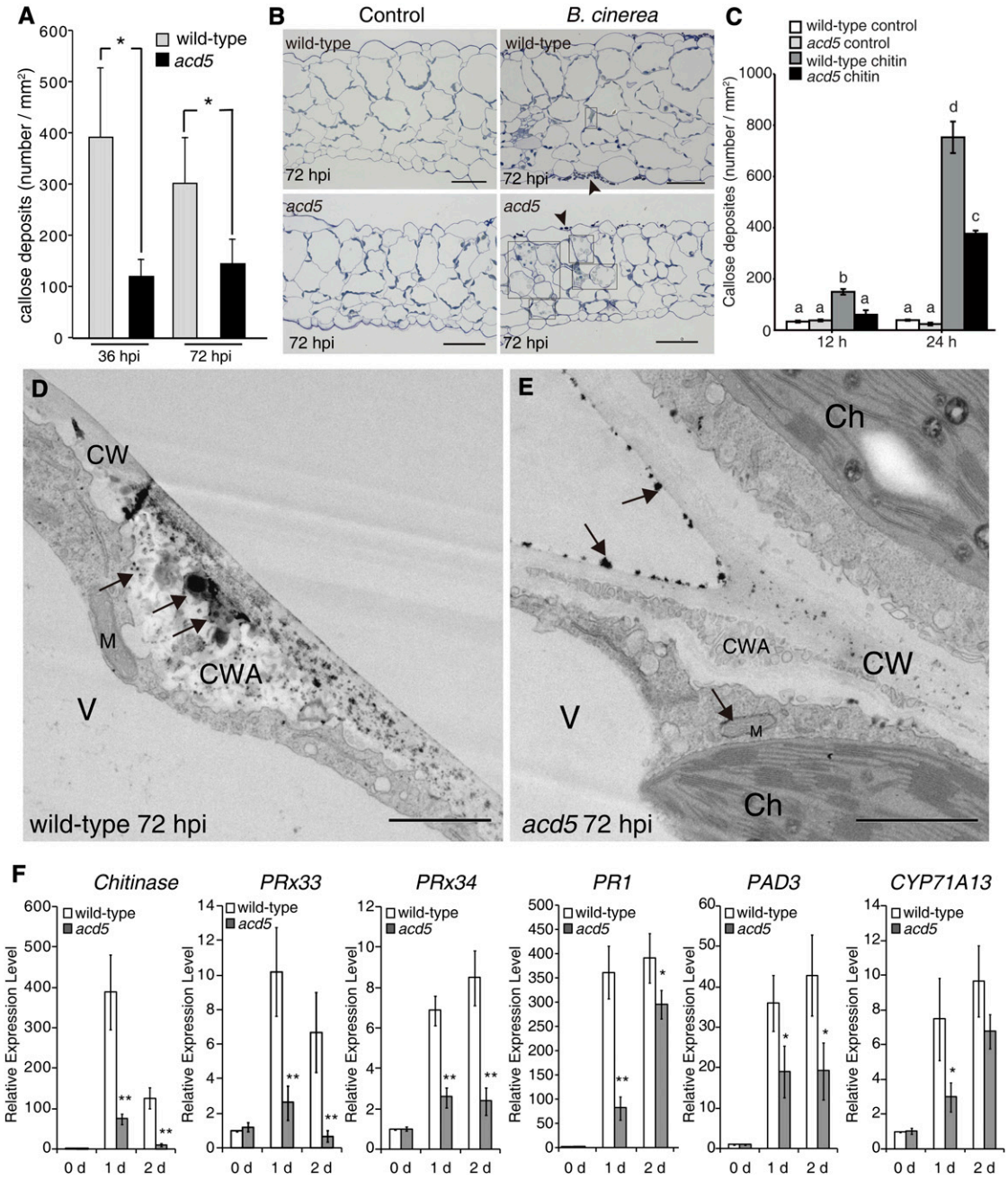

Figure 7. Compromised Defense Responses in *acd5* Plants after *B. cinerea* Infection or Chitin Treatments.

(A) Quantitation of callose deposits in the wild type and *acd5* after inoculation with *B. cinerea* at the indicated times. This experiment was repeated three times with similar results. At least 18 leaves of the wild type or *acd5* were observed in each experiment. Significant differences were determined by Student's *t* test (*P < 0.05). Error bars indicate SD from three independent tests.

(B) Cross sections of wild-type and *acd5* leaves after 2% glucose (control) or *B. cinerea* inoculation for 72 h. Arrowheads indicate pathogen hypha and boxes indicate dead cells. Bars = 50 μm.

(C) Quantitation of callose deposits in the wild type and *acd5* after treated with 100 ng/mL chitin at 12 and 24 h. This experiment was repeated three times with similar results. At least nine leaves of the wild type or *acd5* were observed in each experiment. Letters indicate significantly different values using Fisher's protected least significant difference, a post-hoc multiple *t* test (P < 0.05). Error bars indicate SD from three independent tests.

(D) and **(E)** Electron microscopy images of cell wall appositions of wild-type and *acd5* leaves after *B. cinerea* infection for 72 h. Three different leaf samples of the wild type and *acd5* were observed and two independent experiments were done with similar results. Note the large cell wall apposition (CWA) in wild-type with cerium deposits **(D)** and tiny CWA in *acd5* with free cerium **(E)**. No large size CWA were found in any *acd5* samples. Arrows indicate depositions of cerium. Ch, chloroplast; CW, cell wall; CWA, cell wall apposition; M, mitochondrion; V, vacuole. Bars = 1 μm.

then gradually decreased, and increased again to ~4-fold on the 5th day after infection (Figures 8F to 8H). The individual hydroxyceramides containing long-chain fatty acid increased to higher levels in *acd5* relative to wild-type plants (Figures 8H and 8J; Supplemental Table 8). No significant differences were observed in the other two major sphingolipids, LCBs and glucosylceramides (Figure 8F). These results support the idea that the extent of ceramide accumulation is related to the increased disease symptoms of plants during *B. cinerea* infection.

DISCUSSION

Here, we showed that loss of ceramide kinase has important consequences for both the fate of leaves on older plants and the capacity of leaves on younger plants to effectively activate immune responses during infection with *B. cinerea*. As plants age, the loss of ceramide kinase results in the induction of mitochondrial ROS and autophagy, the abnormal accumulation of ceramides, and premature cell death. In *B. cinerea*-infected younger plants, loss of ceramide kinase causes compromised immune activation at the cell surface, increased disease severity, and accelerated the timing of mitochondrial ROS production and pathogen growth. Thus, key roles for ceramide kinase involve regulating ceramides that affect leaf integrity/survival, ROS, and early pathogen responses at the cell surface. Our data also indicate that accumulation of both long- and very-long-chain ceramides contributes to plant cell death.

Ceramide Kinase Activity and Localization Reflects Its Function

ACD5 protein and ceramide kinase activity are found in multiple compartments of the cell, mainly in membranes. One possibility is that ACD5 is needed in various cell compartments for different biological processes. The highly conserved CXXCXXXC motif in all ceramide kinases is important for enzyme activity and function in plants (Bi et al., 2011) and animals (Lidome et al., 2008); this motif also affects enzyme localization in animal cells (Lidome et al., 2008; Rovina et al., 2009). It is possible that under different stress conditions, ceramide kinase can translocate from one compartment to another, as has been documented in animal cells (Van Overloop et al., 2006; Rovina et al., 2009).

ACD5 also shows modest colocalization with mitochondria. Because the fractionation, immunolocalization, and YFP imaging are in agreement, it seems likely that a pool of ACD5 does reside in mitochondria. The fact that mitochondrial dysfunction is also associated with *acd5* supports the idea that ceramide kinase and specifically the product of the ceramide kinase reaction, Cer-1p, is important for regulating events within mitochondria. This idea is further supported by the observation that ceramide treatment induces a loss in mitochondrial membrane potential that can be mitigated by Cer-1p (Yao et al., 2004). Treatment of plant protoplasts with ceramide also leads to cytochrome C release and programmed cell death (Yao et al., 2004). In animal cells, there appears to be a specific mitochondrial pool of ceramide that is involved in apoptotic cell death (Birbes et al., 2002; Colombini, 2010). A similar role for ceramides may also hold true for plants.

Endogenous Ceramide Accumulation Is a Key Factor in Plant Cell Death

Ceramide accumulation promotes the induction of programmed cell death in plants (Liang et al., 2003; Townley et al., 2005; Wang et al., 2008; Donahue et al., 2010). However, only some types of ceramides (Townley et al., 2005), those with nonhydroxy fatty acyl chain, but not ceramides with 2-hydroxylation, induce cell death in *Arabidopsis* suspension culture cells. Wang et al. (2008) reported that the double mutant *acd5 erh1* (*enhanced RPW8-mediated HR-like cell death*), which affects inositolphosphorylceramide synthase, develops earlier and more severe cell death lesions compared with single mutants. These data support the notion that certain amounts of endogenous ceramide might be needed for cell death induction. Our data indicate that loss of ceramide kinase affects ceramide synthase and putative ceramidase gene expression and results in gradual ceramide accumulation that likely contributes to spontaneous cell death in *acd5* plants. Interestingly, both the *acd5 loh3* and the *acd5 loh2* double mutants show severe cell death before *acd5* shows any cell death phenotype. Because these plants show dramatic increases in long-chain ceramides or very-long-chain ceramides, we infer that not only C16 ceramide accumulation, but also >C18 ceramides contribute to the timing of the *acd5* cell death phenotype. Pathogen-infected plants also show high levels of many ceramide species in both wild-type and *acd5* mutant plants. The current data suggest that maintenance of internal homeostasis of long chain and very long chain ceramides might be important for cell viability.

It is unclear whether in certain mutants or during infection of wild-type plants, ceramides accumulate in specific organelles. One possibility is that some ceramides accumulate in mitochondria, which may contribute to ROS accumulation. Strong mitochondrion-derived ROS occurs in both C2-treated protoplasts and pathogen-infected tissues, supporting the idea that the mitochondrial ROS bursts may result directly from ceramide-mediated mitochondrial damage.

Although we were able to use mass spectrometry to profile and quantify many ceramide species, we were unable with our current methods to reliably detect Cer-1p in our extracts. Possibly this

Figure 7. (continued).

(F) Expression levels of defense-related genes in response to *B. cinerea* in wild-type and *acd5* plants. Defense-related genes assayed were a chitinase family protein (At2g43580), *PRX33*, *PRX34*, *PR1*, *PAD3*, and *CYP71A13*. Total RNA was extracted at the indicated time points for quantitative RT-PCR analysis. *ACT2* was used as an internal control. Gene expression values are presented relative to average wild-type levels at 0 hpi (set as 1). This experiment was repeated three times using independent samples. Values are means ± SD from three biological replicates. Significant differences were determined by Student's *t* test (*P < 0.05 and **P < 0.01).The primers used for these analyses are provided in Supplemental Table 1.
[See online article for color version of this figure.]

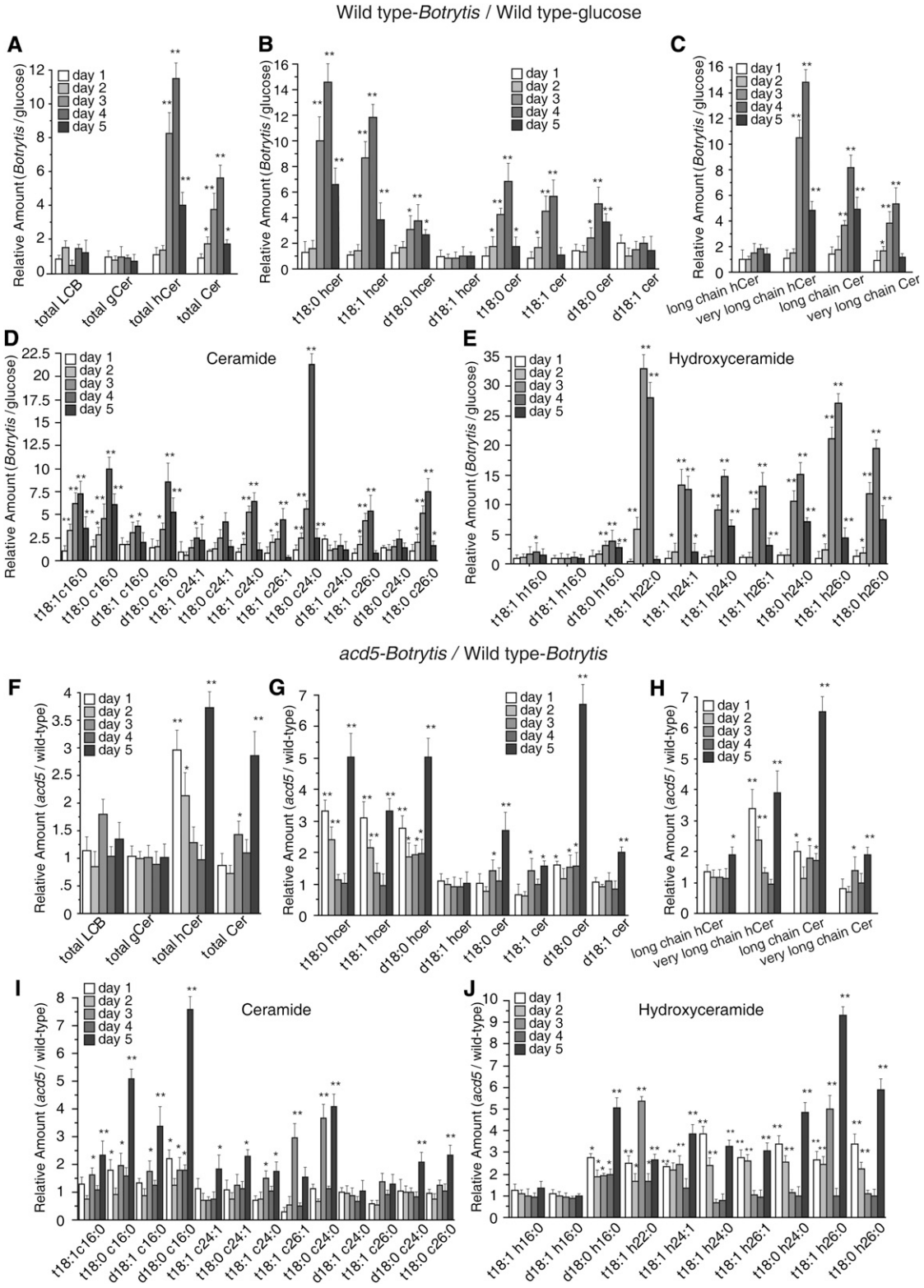

Figure 8. Ceramide Accumulation in Response to *B. cinerea* in Wild-Type and *acd5* Plants.

Three-week-old wild-type and *acd5* plants were sprayed with10^7 spores/mL of *B. cinerea* and sampled at different time points for sphingolipid quantification.

reflects its transient accumulation. Alternatively, Cer-1p may only accumulate in very small amounts, in which case additional purification protocols will be necessary to develop for future studies. Nevertheless, our experiments are consistent with a critical threshold of ceramide accumulation or a certain ratio of Cer/Cer-1p in mediating biotic stress-induced cell death in plants.

Ceramide Accumulation Affects Autophagy

In dark-treated plants, degradation of chloroplasts occurs through autophagic processes (Wada et al., 2009). In yeast, degradation of damaged mitochondria is mediated by an autophagy-related pathway (Okamoto et al., 2009). Recent reports in animal cells indicate that ceramide induces targeting of mitochondria by mitophagy and inhibition of mitochondrial function (Sentelle et al., 2012). It is interesting that *acd5* also shows increased autophagosomes accompanied by ROS generation and mitochondrial-related spontaneous cell death in late development. Autophagy may aide in the removal of damaged material that is generated as a result of ROS accumulation in *acd5*.

Induction of autophagy in plants has been associated with infection and aging (Hayward and Dinesh-Kumar, 2011). Specific signals that can induce autophagy include SA and ROS (Yoshimoto et al., 2009; Hayward and Dinesh-Kumar, 2011). Activation of autophagy in *acd5* coincides with the timing of SA and ROS accumulation (Greenberg et al., 2000; this work). Therefore, autophagy may be activated due to SA and/or ROS production in *acd5* plants. However, it is also possible that ceramides have a more direct role in regulating autophagy, as has been suggested in animal cells (Sentelle et al., 2012).

Ceramide Kinase Affects ROS Production

In *B. cinerea* infections, host susceptibility is positively correlated with the levels of superoxides or H_2O_2 production (Govrin and Levine, 2000). NADPH oxidase-derived ROS limits the spread of cell death after *B. cinerea* infection (Torres et al., 2005). In *acd5* mutants, ROS are affected in several ways, which likely affects several cellular events. During infection, apoplast ROS signals appear later and at lower intensity than in wild-type plants. This likely directly promotes early growth of *B. cinerea*. Thus, at early stages of infection, ceramides at the cell surface, modulated by ceramide kinase, positively regulate apoplast ROS. This ROS appears to have a similar role in early responses to necrotrophs and biotrophs and involves activation of immunity (Mengiste, 2012). However, in *acd5* infections, mitochondrial H_2O_2 occurs earlier and the intensity of ROS accumulation overall increases late in infection. These events may also contribute to the disease process and increased symptom formation. Possibly, ACD5 at the mitochondria is needed to negatively regulate ROS production to suppress the level of cell death.

Ceramide Kinase Regulates Plant Defense Responses

A previous report showed that *acd5* plants accumulate high levels of camalexin and SA in plants with cell death lesions, but not in plants prior to lesion formation (Greenberg et al., 2000). In this study, we used young *acd5* plants, which had not yet manifested the cell death phenotype, for infections with *B. cinerea*. In these plants, *B. cinerea* immediately grows faster and defense responses (gene expression, apoplast ROS, and callose and papillae formation) are reduced or delayed compared with wild-type plants. This result implicates the balance of Cer/Cer-1p or the production of Cer-1p as important in the early activation of plant immunity.

In summary, ceramides that are regulated by ACD5 in cell death control and *Arabidopsis* defense against pathogens. Based on the different defects that loss of ACD5 causes, we propose that ceramide kinase at the plasma membrane regulates cell surface defenses, whereas ceramide kinase at the mitochondria affects the integrity and function of this organelle to suppress cell death. The specific ceramides (or their ratios) that control these functions at different subcellular sites will be a frontier area of research in the future.

METHODS

Plants and Materials

Arabidopsis thaliana wild-type (Columbia) and *acd5* mutant plants (Greenberg et al., 2000) were grown on soil under fluorescent lights as described by Shen et al. (2010). The double mutants *acd5 loh2* and *acd5 loh3* were generated by crossing *acd5* with *loh2* (SALK_018608) or *loh3* (SALK_150849), respectively, and isolated from the F2 progeny by PCR genotyping for T-DNA insertion in *loh2* or *loh3* and sequencing for the point mutation in *acd5* (Supplemental Table 1). The homozygous F3 plants were used for further study.

To generate ACD5 RNAi plants, an artificial microRNA-mediated gene silencing method was performed as previously described (Schwab et al., 2006). In brief, an artificial microRNA precursor was produced by overlapping PCR with pRS300 as a template and specific primers designed using WMD3 software (http://wmd3.weigelworld.org/cgi-bin/webapp.cgi). The fragment containing artificial microRNA precursor was cloned to pCAMBIA1300 under the control of 35S promoter. The resulting plasmid was transformed to wide-type *Arabidopsis* by *Agrobacterium tumefaciens* strain EHA105 (Zhang et al., 2006). Transgenic plants were selected by hygromycin selection, and T2 plants were used for further study. The primers are shown in Supplemental Table 1.

Figure 8. (continued).

(A) to **(E)** Relative level of sphingolipids in infected wild type versus 2% glucose controls (set to 1).
(F) to **(J)** Relative level of sphingolipids in infected *acd5* versus infected wild type (set to 1). Measurements were of four major sphingolipid classes (**[A]** and **[F]**), ceramide and hydroxyceramide containing various LCBs (**[B]** and **[G]**), ceramide and hydroxyceramide containing various acyl lengths (**[C]** and **[H]**), individual ceramide species (**[D]** and **[I]**), and individual hydroxyceramide species (**[E]** and **[J]**). Significant differences were determined by Student's *t* test (*$P < 0.05$ and **$P < 0.01$) (see Supplemental Tables 7 and 8 for the absolute values). Means ± SD are shown from three independent experiments.

N-acetoyl-D-erythro-sphingosine (C2 ceramide; product number 860502P), *N*-octanoyl-D-erythro-sphingosine (C8 ceramide; product number 860508P), *N*-acetoyl-ceramide-1-phosphate (C2-1-phosphate; product number 860530P) ceramides, and 1′,3′-bis[1,2-dimyristoyl-sn-glycero-3-phospho]-sn-glycerol (cardiolipin; product number 710332) were purchased from Avanti Polar Lipids. Octyl β-glucoside (product number 28310) was purchased from Pierce Biotechnology. [γ-^{32}P]ATP (3000 Ci/mmole) (product number AA0068) was from Amersham Biosciences. *N*-acetyl-cysteine (product number A7250) was purchased from Sigma-Aldrich. Protein kinase inhibitor K252a was purchased from Calbiochem EMD Biosciences (product number 420297). Protease inhibitor for plant cells was purchased from Sigma-Aldrich (product number P9599).

Protoplast Isolation and Treatments

For chemical treatments, protoplasts were made according to the procedure of Shen et al. (2010). The viability was determined by fluorescein diacetate staining (Liang et al., 2003).

For transient expression, protoplasts were isolated from leaves of 25-d-old *Arabidopsis* wild-type plants as described previously, with several changes (Wu et al., 2009). The upper and lower epidermal surfaces were stabilized by affixing a strip of yellow 3M tape and a strip of transparent 3M tape, respectively. The translucent tape was then carefully pulled away from the yellow tape, peeling away the lower epidermal surface cell layer. The peeled leaves, still adhering to the yellow tape, were transferred to a Petri dish containing ~10 mL of enzyme mixture (1.2% [w/v] cellulase R10 and 0.3% [w/v] Macerozyme R10 [Yakult Pharmaceutical], 0.5 M mannitol, 20 mM KCl, 20 mM MES, 10 mM $CaCl_2$, 5 mM mercaptoethanol, and 0.1% [w/v] BSA adjusted to pH 5.7 with KOH). The leaves were gently shaken (40 rpm on a platform shaker) in the light for 60 min. Then protoplasts were passed through a 40-μm nylon mesh and collected after washing twice with W5 media (154 mM NaCl, 125 mM $CaCl_2$, 5 mM KCl, 2 mM MES, and 5 mM glucose adjusted to pH 5.7 with KOH) and stored at 4°C for transformation.

Plasmid Construction and Transient Expression

To generate the *ACD5:YFP* construct, the full-length *ACD5* open reading frame without a stop codon was amplified with the follower primer set including *Sal*I and *Bam*HI restriction sites: forward (5′-ACGCGTCGACATGGAGGAAGGTCGTGACGAC-3′) and reverse (5′-CGCGGATCCTTTTATCTCTGGACCAGATGCGAAC-3′), respectively. The PCR product was subcloned in frame with PA7-YFP (constructed from the pUC18 backbone) after *Sal*I and *Bam*HI double digestion. The P35S:ACD5:YFP plasmid was coexpressed with an ER marker plasmid and a plasma membrane or a Golgi marker plasmid by transient expression in protoplasts. Protoplast transfection was performed as described previously (Yoo et al., 2007). The transfected protoplasts were cultured in weak light (~5 μmol photons·m^2·s^{-1}) for 16 to 24 h at room temperature before confocal microscopy. Three independent repeat experiments were done with similar results and at least 10 fields in each experiment were observed. The images were taken with a confocal laser scanning microscope (Leica TCS SP5 AOBS).

Fungal Culture and Infection

The *Botrytis cinerea* (strain NJ-09, obtained from Xili Liu in China Agriculture University) was cultured on potato dextrose agar (1000 mL distilled water, 300 g potatoes, 20 g glucose, and 15 g agar) and incubated at 25°C in the dark. Conidia were collected in distilled water and gentle shaken for 45 min in room temperature. After filtering with four to six layers of gauze, the spores were washed twice with distilled water and then resuspended in 2% glucose for inoculation. For plant inoculation, the fungal spore density was adjusted to 1×10^7 spores mL^{-1} in 2% glucose and sprayed on 20-d-old plants. Inoculated plants were kept under a transparent cover to maintain high humidity and transferred to an illuminated incubator. After incubation for 24 h in the dark, the plants were cultured with 16-h light at ~75 μmol photons·m^2·s^{-1} and an 8-h dark cycle.

Histochemical Assays

Trypan blue staining to visualize cell death and conidial germination were performed as previously described (Rate et al., 1999) with minor modifications. Fresh tissue was harvested, stained, and boiled for 30 s in lactophenol (10 mL of lactic acid, 10 mL of glycerol, 10 mL of liquid phenol, and 10 mL of distilled water) containing 10 mg of trypan blue. Tissue was rapidly transferred and boiled in alcoholic lactophenol (2:1 95% ethanol: lactophenol) for 1 min, washed in 50% ethanol at room temperature for 2 min, and stored in water. The stained leaves were examined using a fluorescence microscope (Carl Zeiss) with a CCD camera (AxioCam HRc; Carl Zeiss). The germination rate was counted and the length of fungal hyphae was measured using Leica LAS software. The experiments were repeated at least three times with similar results and over 100 spores and hyphae were counted in each experiment.

The presence of ROS in leaf samples was determined as previously described (Watanabe and Lam, 2006). The DAB-stained leaves were observed under a stereomicroscope (SteREO Lumar.V12; Carl Zeiss) equipped with a CCD camera (AxioCam MRc). Data were analyzed using ImageJ software as described previously (Yoshimoto et al., 2009). The final measurement used to quantify the DAB staining was the area of the stain divided by the total area of the leaf. At least 18 leaves per genotype were quantified each time and three independent tests were done.

Callose staining was done as previously described (Watanabe and Lam, 2006) with several changes. Fresh leaves were fixed in FAA solution (2:1:9:8 formaldehyde:acetic acid:ethanol:water) and boiled in alcoholic lactophenol (2:1 95% ethanol:lactophenol) for 2 to 3 min. The leaves were washed in 50% ethanol for 2 min, rinsed in distilled water, stained overnight in aniline blue (0.01% aniline blue powder in 150 mM K_2HPO_4, pH 9.5), and then stored in 50% glycerol. Callose deposition was visualized under an epifluorescence microscope (Axio Imager A1; Carl Zeiss) equipped with a 4′,6-diamidino-2-phenylindole filter set (excitation 365 nm, emission 445/50 nm, and dichroic 395 nm). For the chitin-induced callose assay, 25-d-old wild-type and *acd5* plant leaves were inoculated by syringe infiltration with 100 ng/mL chitin (Sigma-Aldrich), collected at 12 and 24 hpi and stained as above. The quantification of callose in inoculated leaves was performed using Imaris software version 7.0.0 (Bitplane) under a ×10 objective. The experiments were repeated three times and at least 12 leaves in each treatment were used for quantification.

Antibody Generation and Immunoblotting

A polypeptide from ACD5 protein (amino acids from 249 to 451) was expressed to generate antibody. The protein expression, immunizations, and antiserum purifications were performed (Abmart). Briefly, the expression vector including the corresponding fragment of *ACD5* was transformed into the *Escherichia coli* expression strain BL21 (Abmart). The expression of recombinant protein was induced and the bacterial cells were harvested, ruptured using sonication, and purified by nickel column chromatography. One milliliter of purified antigen was injected subcutaneously into the flanks of one rabbit. Booster doses were injected at 2, 4, and 6 weeks after the initial injection using Freund's incomplete adjuvant. Whole blood was collected from anesthetic rabbit by cardiac puncture 2 weeks after last injection. The serum was collected from clotted blood and purified by Protein A column. The titer of antiserum was determined by ELISA.

Anti-ACD5 antiserum was used for immunoblotting at a concentration of 1:500 in TBST buffer (25 mM Tris-HCl, pH 7.4, 140 mM NaCl, 0.1% [w/v] Tween 20, and 5% nonfat dry milk) and detected by horseradish peroxidase-conjugated goat anti-rabbit antibody (1:5000; Jackson) followed by a ECL Plus Kit as the manufacturer's instructions (Bio-Rad

Laboratories). By calculating the ratio of intensity of ACD5 bands to Coomassie Brilliant Blue-stained Rubisco (RBC) large subunits, the relative protein expression value was determined according to the wild type (set as 1). Immunoblotting and quantification analysis were performed for at least three biological replications.

Ceramide Kinase Activity Assays

Ceramide kinase activity assay of each cell compartment (Supplemental Figures 1G and 1H) was measured as described previously (Liang et al., 2003) with C8-ceramide as the substrate. C8 ceramide was resuspended in micelles (15 mg cardiolipin, 150 mg β-octylglucoside, 20 μL 0.1 M DETAPAC, pH 6.6, in 1980 μL of water) and subjected to ceramide kinase reactions using various cell extracts/fractions. The final composition of the reaction was: 0.8 μM ATP, 50 mM Tris, pH 8.3, 1 mM DTT, 2 mM EGTA, 3 mM $CaCl_2$, 0.5 mM $MgCl_2$, 20 μL lipids, 2 μg of cell extracts/fractions, and 1 μL [α-^{32}P]ATP (3000 Ci/mmole) in 100 μL total volume. The reactions were incubated at 37°C for 30 min and terminated by adding 600 μL of chloroform:methanol 1:1 and 265 μL of 1 M KCl in 20 mM MOPS, pH 7.2. The mixtures were centrifuged for 1 min, and lower phases were collected and dried in a fume hood overnight. The lipids were resuspended in 10 μL chloroform and separated using thin layer chromatography plates (silica gel 60 by EMD) with water:acetic acid:methanol:acetone:chloroform 5:10:15:20:50. The thin layer chromatography plates were exposed to a phosphor imaging screen and quantified by ImageQuant program.

Membrane and Cellular Fractionation and Immunoblots

For membrane fractionation (Supplemental Figures 1G and 1H), 3-week-old greenhouse grown plants were homogenized by mortar and pestle in 2× homogenizing buffer (100 mm Tris-HCl, pH 7.5, 250 mm sucrose, 10 mm EDTA, 2 mm EGTA, and protease inhibitor cocktail). The homogenates were cleared initially by filtering through two layers of Miracloth, then subjected to a series of centrifugation steps, according to Ahmed et al. (1997). In short, after an initial spin at 5000 rpm for 10 min, the supernatant was centrifuged at 17,000*g* for 30 min to obtain a pellet enriched in microsomal membranes. The supernatant of the above spin was centrifuged again at 100,000*g* for 1 h to pellet plasma membranes. The fractions were verified for their contents by immunoblot with mitochondrial NAD9 and plasma membrane H^+-ATPase (PM) antibody markers.

Further purification of plasma membrane was conducted according to Lu et al. (2005). The final pellets were resuspended in ceramide kinase extraction buffer. The fractions were verified by antibody markers for plasma membrane H^+-ATPase (PMA2), ER H^+-ATPase (ACA2), and Golgi α-mannosidase. Mitochondrial purification was done according to Schwitzguebel and Siegenthaler (1984). Mitochondrial cytochrome C oxidase assay was also used to verify the fractions containing mitochondria.

Transmission Electron Microscopy

Subcellular localization of hydrogen peroxide was determined based on the generation of cerium perhydroxides as described previously (Yao et al., 2002). Ultrathin sections (90 nm) were obtained on a microtome (Leica EM UC6) using a diamond knife (Diatome) and examined without staining. The images were obtained using a transmission electron microscope (JEM-1400; JEOL) at an accelerating voltage of 120 kV.

For immunoelectron microscopy, ultrathin sections were cut and collected on nickel grids as described (Yao and Greenberg, 2006). Sections were incubated with the anti-ACD5 antiserum at a concentration of 1:40 (ACD5 polyclonal antibody prepared by Abmart Company) for 2 h at room temperature. Goat-anti-rabbit IgG labeled with 10-nm colloidal gold (Electron Microscopy Sciences) was used for bound primary antibody. Specimens were stained with uranyl acetate and lead citrate before observation under a transmission electron microscope (JEM-1400; JEOL) at an accelerating voltage of 120 kV. For statistical analysis of ACD5 localization, 20 ultrathin cross sections of the samples were prepared from three different blocks. At least 20 cells were photographed and analyzed in each of the treatments.

Quantitative RT-PCR Analysis

Total RNA was isolated using E.Z.N.A. plant RNA kit (R6827-01) according to the manufacturer's instructions (Omega Bio-tek). For each sample, 1 μg RNA was reverse transcribed into cDNA using PrimeScript RT reagent kit with gDNA Eraser (TAKARA). A total of 4.6 μL of diluted cDNA samples (1:15) was mixed with 5 μL 2× SYBR Premix Ex Taq II (TAKARA) and 0.4 μL gene-specific primers in 384-well plates (Roche) and then quantitatively analyzed by LightCycler480 real-time PCR system (Roche). Three biological replicates were performed for each template and primer combination, and *ACT2* expression level was used as the internal control. The $2^{-\Delta\Delta CT}$ method (Livak and Schmittgen, 2001) was used to calculate the relative expression level of target genes according to the expression level of *ACT2*. The primers for amplification are listed in Supplemental Table 1.

Sphingolipid Analysis

Measurement of sphingolipids was performed by electrospray ionization tandem mass spectrometry analysis on an Agilent 6410 triple quadrupole mass spectrometer, operating in multiple reaction monitoring positive ionization mode as described by Markham and Jaworski (2007). Briefly, 30 mg of lyophilized samples was homogenized. The internal standards (C_{17} base D-erythro-sphingosine and C12-Ceramide) were added and extracted with the isopropanol/hexane/water (55:20:25 v/v/v). After incubation at 60°C for 15 min, the supernatants were dried by nitrogen. The dried extract was deesterified by dissolving in 2 mL of 33% methylamine solution in ethanol/water (7:3 v/v) and incubated at 50°C for 1 h. After being dried with nitrogen, the sample was dissolved in 1 mL of methanol. The samples were injected on the Agilent 1200/6410QQQ LC/MS system and gradient-eluted from the Agilent XDB C8, 50 × 2.1-mm, 1.8-μm particle size column. Peaks corresponding to the target analytics and internal standards were collected and processed using the Agilent Masshunter Quantitative Analysis software. The components of sphingolipids were determined as described previously (Markham and Jaworski, 2007).

ROS Production Observation

Microscopy in Figure 2E and Supplemental Figure 2 was performed using a confocal laser scanning microscope system (Leica TCS SP2 AOBS) as described previously (Yao and Greenberg, 2006).

Generation of *acd5*/*GFP-ATG8* Plants and Confocal Microscopy

To generate the *acd5*/*GFP-ATG8e* plants, the *acd5* mutants were crossed to GFP-ATG8e (Xiao et al., 2010). The *acd5*/*GFP-ATG8e* homozygous plants were obtained by screening F2 seeds to identify the *acd5* phenotype and confirmed by PCR. For microscopy observation, GFP-ATG8e and *acd5*/*GFP-ATG8e* plants were grown on normal conditions for 1 d after infiltrating leaves with 1 μM concanamycin A (WAKO). The infiltrated leaves were detached and then observed under confocal microscope (Leica TCS SP5 AOBS). For autophagosome (green vesicles) statistical analysis, fields (80 μm × 80 μm × 40 μm) on each leaf were randomly selected and captured using *z* axis scan. At least 12 leaves were observed in each treatment. Images were processed using Imaris 7.0 software.

Accession Numbers

Sequence data from this article can be found in the GenBank/EMBL database or the Arabidopsis Genome Initiative database under the

following accession numbers: *ACT2* (At3g18780), *ATG3* (AT5G61500), *ATG7* (AT5G45900), *ATG8a* (AT4G21980), *ATG8e* (AT2G45170), *ATG8g* (AT3G60640), *ATG8 h* (AT3G06420), chitinase family protein (AT2g43580), *CYP71A13* (AT2G30770), *PAD3* (AT3G26830), *PR1* (AT2G14610), *PRX33* (AT3g49110), *PRX34* (AT3g49120), putative ceramidase genes (*At1g07380*, *At2g38010*, and *At5g58980*), the three ceramide synthetase genes *LOH1* (At3G25540), *LOH2* (At3G19260), and *LOH3* (At1G13580), *IPCD* (At4g29680, At4g29690, and At4g29700), *IPCS* (At2g37940, At2g29525, and At3g54020), *GCD* (At3g24180, At4g10060, At1g33700, and At5g49900), *CES1* (At4g22330), and *GCS* (At2g19880). Germplasm used *acd5* (Greenberg et al., 2000), *loh2* (SALK_018608), and *loh3* (SALK_150849).

Supplemental Data

The following materials are available in the online version of this article.

Supplemental Figure 1. ACD5 Localization.

Supplemental Figure 2. Several Types of Treatments Block ROS Production Induced by C2-Ceramide

Supplemental Figure 3. Relative Contents of LCBs and Glucosylceramides during *acd5* Development.

Supplemental Figure 4. Expression Levels of Sphingolipid Metabolism Genes in *acd5* and Wild-Type Plants.

Supplemental Figure 5. Expression of *ACD5* during Development and *Botrytis* Infection in Wild-Type Plants.

Supplemental Figure 6. The Effect of *loh2* on the Visible Phenotype and Ceramide Contents of *acd5* Plants.

Supplemental Figure 7. Increased Symptoms in *acd5* after Infection with *Botrytis*.

Supplemental Figure 8. Callose Depositions in Wild-Type and *acd5* Leaves after *Botrytis cinerea* Infection or Chitin Treatments.

Supplemental Table 1. Primers for qPCR Used in This Study.

Supplemental Table 2. Measurement of Ceramides in Wild-Type and *acd5* Leaves.

Supplemental Table 3. Measurement of Hydroxyceramides in Wild-Type and *acd5* Leaves.

Supplemental Table 4. Measurement of Total Sphingolipids in 25-d-Old Wild-Type, *acd5*, *loh3*, and *acd5 loh3* Leaves.

Supplemental Table 5. Measurement of Ceramides in 25-d-Old Wild-Type, *acd5*, *loh3*, and *acd5 loh3* Leaves.

Supplemental Table 6. Measurement of Ceramides in 35-d-Old Wild-Type, *acd5*, *loh2*, and *acd5 loh2* Leaves.

Supplemental Table 7. Measurement of Sphingolipids in Wild-Type Plants Challenged by 2% Glucose or *Botrytis* for 1 to 5 Days.

Supplemental Table 8. Measurement of Sphingolipids in Wild-Type and *acd5* after *Botrytis* Infection for 1 to 5 Days.

ACKNOWLEDGMENTS

We thank M. Boutry, J. Harper, S. Bednarek, and J. M. Grienenberger for the gift of antibodies against plasma membrane H^+-ATPase (PM), ER H^+-ATPase (ACA2), Golgi α-mannosidase, and mitochondrial NAD9, respectively. We also thank Shi Xiao for supplying GFP-ATG8e seeds, Detlef Weigel for supplying the pRS300 vector, the ABRC for providing *Arabidopsis* T-DNA insertion lines and organelle markers, and Meng-hua Liu for assistance with sphingolipid analysis. This work was supported by the National Key Basic Science 973 Program (2012CB114006), the National Natural Science Foundation of China (31170247), the Fundamental Research Funds for the Central Universities (13lgjc27) to N.Y., the China Postdoctoral Science Foundation (2011M501357) to F.-C.B., and National Institutes of Health Grant R01 GM54292 to J.T.G.

AUTHOR CONTRIBUTIONS

N.Y., F.-C.B., H.L., and J.T.G. conceived and designed the experiments. F.-C.B., Z.L., J.-X.W., H.L., X.-L.X., C.F., J.Y., T.-J.S., G.-Y.D., C.R., and N.Y. performed the experiments. F.-C.B., N.Y., Z.L., and J.T.G. analyzed the data. N.Y., J.T.G., and W.-W.S. contributed reagents/materials/analysis tools. N.Y., J.T.G., and F.-C.B. wrote the article.

Received April 24, 2014; revised June 12, 2014; accepted August 4, 2014; published August 22, 2014.

REFERENCES

Abbas, H.K., Tanaka, T., Duke, S.O., Porter, J.K., Wray, E.M., Hodges, L., Sessions, A.E., Wang, E., Merrill, A.H., Jr., and Riley, R.T. (1994). Fumonisin- and AAL-toxin-induced disruption of sphingolipid metabolism with accumulation of free sphingoid bases. Plant Physiol. **106:** 1085–1093.

Ahmed, S.U., Bar-Peled, M., and Raikhel, N.V. (1997). Cloning and subcellular location of an *Arabidopsis* receptor-like protein that shares common features with protein-sorting receptors of eukaryotic cells. Plant Physiol. **114:** 325–336.

Arana, L., Gangoiti, P., Ouro, A., Trueba, M., and Gómez-Muñoz, A. (2010). Ceramide and ceramide 1-phosphate in health and disease. Lipids Health Dis. **9:** 15.

Asai, T., Stone, J.M., Heard, J.E., Kovtun, Y., Yorgey, P., Sheen, J., and Ausubel, F.M. (2000). Fumonisin B1-induced cell death in *arabidopsis* protoplasts requires jasmonate-, ethylene-, and salicylate-dependent signaling pathways. Plant Cell **12:** 1823–1836.

Bi, F.C., Zhang, Q.F., Liu, Z., Fang, C., Li, J., Su, J.B., Greenberg, J.T., Wang, H.B., and Yao, N. (2011). A conserved cysteine motif is critical for rice ceramide kinase activity and function. PLoS ONE **6:** e18079.

Birbes, H., El Bawab, S., Obeid, L.M., and Hannun, Y.A. (2002). Mitochondria and ceramide: intertwined roles in regulation of apoptosis. Adv. Enzyme Regul. **42:** 113–129.

Chen, M., Cahoon, E., Saucedo-García, M., Plasencia, J., and Gavilanes-Ruíz, M. (2009). Plant sphingolipids: structure, synthesis and function. In Lipids in Photosynthesis: Essential and Regulatory Functions, H. Wada and N. Murata, eds (Dordrecht, The Netherlands: Springer), pp. 77–116.

Colombini, M. (2010). Ceramide channels and their role in mitochondria-mediated apoptosis. Biochim. Biophys. Acta **1797:** 1239–1244.

Daudi, A., Cheng, Z., O'Brien, J.A., Mammarella, N., Khan, S., Ausubel, F.M., and Bolwell, G.P. (2012). The apoplastic oxidative burst peroxidase in Arabidopsis is a major component of pattern-triggered immunity. Plant Cell **24:** 275–287.

de Jonge, R., van Esse, H.P., Kombrink, A., Shinya, T., Desaki, Y., Bours, R., van der Krol, S., Shibuya, N., Joosten, M.H.A.J., and Thomma, B.P.H.J. (2010). Conserved fungal LysM effector Ecp6 prevents chitin-triggered immunity in plants. Science **329:** 953–955.

Donahue, J.L., Alford, S.R., Torabinejad, J., Kerwin, R.E., Nourbakhsh, A., Ray, W.K., Hernick, M., Huang, X., Lyons, B.M., Hein, P.P., and Gillaspy, G.E. (2010). The *Arabidopsis thaliana Myo*-inositol 1-phosphate synthase1 gene is required for *Myo*-inositol synthesis and suppression of cell death. Plant Cell **22:** 888–903.

Govrin, E.M., and Levine, A. (2000). The hypersensitive response facilitates plant infection by the necrotrophic pathogen *Botrytis cinerea.* Curr. Biol. **10:** 751–757.

Greenberg, J.T., Silverman, F.P., and Liang, H. (2000). Uncoupling salicylic acid-dependent cell death and defense-related responses from disease resistance in the *Arabidopsis* mutant *acd5.* Genetics **156:** 341–350.

Hannun, Y.A., and Luberto, C. (2000). Ceramide in the eukaryotic stress response. Trends Cell Biol. **10:** 73–80.

Hannun, Y.A., and Obeid, L.M. (2008). Principles of bioactive lipid signalling: lessons from sphingolipids. Nat. Rev. Mol. Cell Biol. **9:** 139–150.

Hayward, A.P., and Dinesh-Kumar, S.P. (2011). What can plant autophagy do for an innate immune response? Annu. Rev. Phytopathol. **49:** 557–576.

Liang, H., Yao, N., Song, J.T., Luo, S., Lu, H., and Greenberg, J.T. (2003). Ceramides modulate programmed cell death in plants. Genes Dev. **17:** 2636–2641.

Lidome, E., Graf, C., Jaritz, M., Schanzer, A., Rovina, P., Nikolay, R., and Bornancin, F. (2008). A conserved cysteine motif essential for ceramide kinase function. Biochimie **90:** 1560–1565.

Livak, K.J., and Schmittgen, T.D. (2001). Analysis of relative gene expression data using real-time quantitative PCR and the $2^{(-\Delta\ \Delta\ C(T))}$ Method. Methods **25:** 402–408.

Lu, H., Liu, Y., and Greenberg, J.T. (2005). Structure-function analysis of the plasma membrane-localized Arabidopsis defense component ACD6. Plant J. **44:** 798–809.

Markham, J.E., and Jaworski, J.G. (2007). Rapid measurement of sphingolipids from *Arabidopsis thaliana* by reversed-phase high-performance liquid chromatography coupled to electrospray ionization tandem mass spectrometry. Rapid Commun. Mass Spectrom. **21:** 1304–1314.

Mengiste, T. (2012). Plant immunity to necrotrophs. Annu. Rev. Phytopathol. **50:** 267–294.

Okamoto, K., Kondo-Okamoto, N., and Ohsumi, Y. (2009). Mitochondria-anchored receptor Atg32 mediates degradation of mitochondria via selective autophagy. Dev. Cell **17:** 87–97.

Pattanayak, G.K., Venkataramani, S., Hortensteiner, S., Kunz, L., Christ, B., Moulin, M., Smith, A.G., Okamoto, Y., Tamiaki, H., Sugishima, M., and Greenberg, J.T. (2012). Accelerated cell death 2 suppresses mitochondrial oxidative bursts and modulates cell death in Arabidopsis. Plant J. **69:** 589–600.

Peer, M., Stegmann, M., Mueller, M.J., and Waller, F. (2010). *Pseudomonas syringae* infection triggers *de novo* synthesis of phytosphingosine from sphinganine in *Arabidopsis thaliana.* FEBS Lett. **584:** 4053–4056.

Rate, D.N., Cuenca, J.V., Bowman, G.R., Guttman, D.S., and Greenberg, J.T. (1999). The gain-of-function Arabidopsis acd6 mutant reveals novel regulation and function of the salicylic acid signaling pathway in controlling cell death, defenses, and cell growth. Plant Cell **11:** 1695–1708.

Rovina, P., Schanzer, A., Graf, C., Mechtcheriakova, D., Jaritz, M., and Bornancin, F. (2009). Subcellular localization of ceramide kinase and ceramide kinase-like protein requires interplay of their Pleckstrin Homology domain-containing N-terminal regions together with C-terminal domains. Biochim. Biophys. Acta **1791:** 1023–1030.

Saucedo-García, M., Guevara-García, A., González-Solís, A., Cruz-García, F., Vázquez-Santana, S., Markham, J.E., Lozano-Rosas, M.G., Dietrich, C.R., Ramos-Vega, M., Cahoon, E.B., and Gavilanes-Ruíz, M. (2011). MPK6, sphinganine and the LCB2a gene from serine palmitoyltransferase are required in the signaling pathway that mediates cell death induced by long chain bases in *Arabidopsis.* New Phytol. **191:** 943–957.

Schwab, R., Ossowski, S., Riester, M., Warthmann, N., and Weigel, D. (2006). Highly specific gene silencing by artificial microRNAs in *Arabidopsis.* Plant Cell **18:** 1121–1133.

Schwitzguebel, J.P., and Siegenthaler, P.A. (1984). Purification of peroxisomes and mitochondria from spinach leaf by percoll gradient centrifugation. Plant Physiol. **75:** 670–674.

Sentelle, R.D., Senkal, C.E., Jiang, W., Ponnusamy, S., Gencer, S., Selvam, S.P., Ramshesh, V.K., Peterson, Y.K., Lemasters, J.J., Szulc, Z.M., Bielawski, J., and Ogretmen, B. (2012). Ceramide targets autophagosomes to mitochondria and induces lethal mitophagy. Nat. Chem. Biol. **8:** 831–838.

Shen, C.X., Zhang, Q.F., Li, J., Bi, F.C., and Yao, N. (2010). Induction of programmed cell death in *Arabidopsis* and rice by single-wall carbon nanotubes. Am. J. Bot. **97:** 1602–1609.

Shi, L., Bielawski, J., Mu, J., Dong, H., Teng, C., Zhang, J., Yang, X., Tomishige, N., Hanada, K., Hannun, Y.A., and Zuo, J. (2007). Involvement of sphingoid bases in mediating reactive oxygen intermediate production and programmed cell death in *Arabidopsis.* Cell Res. **17:** 1030–1040.

Ternes, P., Feussner, K., Werner, S., Lerche, J., Iven, T., Heilmann, I., Riezman, H., and Feussner, I. (2011). Disruption of the ceramide synthase LOH1 causes spontaneous cell death in *Arabidopsis thaliana.* New Phytol. **192:** 841–854.

Thomma, B.P.H.J., Nelissen, I., Eggermont, K., and Broekaert, W.F. (1999). Deficiency in phytoalexin production causes enhanced susceptibility of *Arabidopsis thaliana* to the fungus *Alternaria brassicicola.* Plant J. **19:** 163–171.

Torres, M.A., Jones, J.D., and Dangl, J.L. (2005). Pathogen-induced, NADPH oxidase-derived reactive oxygen intermediates suppress spread of cell death in *Arabidopsis thaliana.* Nat. Genet. **37:** 1130–1134.

Townley, H.E., McDonald, K., Jenkins, G.I., Knight, M.R., and Leaver, C.J. (2005). Ceramides induce programmed cell death in *Arabidopsis* cells in a calcium-dependent manner. Biol. Chem. **386:** 161–166.

Van Baarlen, P., Staats, M., and VAN Kan, J.A. (2004). Induction of programmed cell death in lily by the fungal pathogen *Botrytis elliptica.* Mol. Plant Pathol. **5:** 559–574.

Van Baarlen, P., Woltering, E.J., Staats, M., and VAN Kan, J.A. (2007). Histochemical and genetic analysis of host and non-host interactions of *Arabidopsis* with three *Botrytis* species: an important role for cell death control. Mol. Plant Pathol. **8:** 41–54.

Van Overloop, H., Gijsbers, S., and Van Veldhoven, P.P. (2006). Further characterization of mammalian ceramide kinase: substrate delivery and (stereo)specificity, tissue distribution, and subcellular localization studies. J. Lipid Res. **47:** 268–283.

Wada, S., Ishida, H., Izumi, M., Yoshimoto, K., Ohsumi, Y., Mae, T., and Makino, A. (2009). Autophagy plays a role in chloroplast degradation during senescence in individually darkened leaves. Plant Physiol. **149:** 885–893.

Wang, W., Jones, C., Ciacci-Zanella, J., Holt, T., Gilchrist, D.G., and Dickman, M.B. (1996). Fumonisins and *Alternaria alternata lycopersici* toxins: sphinganine analog mycotoxins induce apoptosis in monkey kidney cells. Proc. Natl. Acad. Sci. USA **93:** 3461–3465.

Wang, W., et al. (2008). An inositolphosphorylceramide synthase is involved in regulation of plant programmed cell death associated with defense in *Arabidopsis.* Plant Cell **20:** 3163–3179.

Watanabe, N., and Lam, E. (2006). Arabidopsis Bax inhibitor-1 functions as an attenuator of biotic and abiotic types of cell death. Plant J. **45:** 884–894.

Wu, F.H., Shen, S.C., Lee, L.Y., Lee, S.H., Chan, M.T., and Lin, C.S. (2009). Tape-*Arabidopsis* Sandwich - a simpler *Arabidopsis* protoplast isolation method. Plant Methods **5:** 16.

Xiao, S., Gao, W., Chen, Q.F., Chan, S.W., Zheng, S.X., Ma, J., Wang, M., Welti, R., and Chye, M.L. (2010). Overexpression of

Arabidopsis acyl-CoA binding protein ACBP3 promotes starvation-induced and age-dependent leaf senescence. Plant Cell **22:** 1463–1482.

Yao, N., and Greenberg, J.T. (2006). *Arabidopsis ACCELERATED CELL DEATH2* modulates programmed cell death. Plant Cell **18:** 397–411.

Yao, N., Eisfelder, B.J., Marvin, J., and Greenberg, J.T. (2004). The mitochondrion—an organelle commonly involved in programmed cell death in *Arabidopsis thaliana.* Plant J. **40:** 596–610.

Yao, N., Tada, Y., Sakamoto, M., Nakayashiki, H., Park, P., Tosa, Y., and Mayama, S. (2002). Mitochondrial oxidative burst involved in apoptotic response in oats. Plant J. **30:** 567–579.

Yoo, S.-D., Cho, Y.-H., and Sheen, J. (2007). Arabidopsis mesophyll protoplasts: a versatile cell system for transient gene expression analysis. Nat. Protoc. **2:** 1565–1572.

Yoshimoto, K., Hanaoka, H., Sato, S., Kato, T., Tabata, S., Noda, T., and Ohsumi, Y. (2004). Processing of ATG8s, ubiquitin-like proteins, and their deconjugation by ATG4s are essential for plant autophagy. Plant Cell **16:** 2967–2983.

Yoshimoto, K., Jikumaru, Y., Kamiya, Y., Kusano, M., Consonni, C., Panstruga, R., Ohsumi, Y., and Shirasu, K. (2009). Autophagy negatively regulates cell death by controlling NPR1-dependent salicylic acid signaling during senescence and the innate immune response in *Arabidopsis.* Plant Cell **21:** 2914–2927.

Zhang, X., Henriques, R., Lin, S.S., Niu, Q.W., and Chua, N.H. (2006). Agrobacterium-mediated transformation of Arabidopsis thaliana using the floral dip method. Nat. Protoc. **1:** 641–646.

Zhou, R., Yazdi, A.S., Menu, P., and Tschopp, J. (2011). A role for mitochondria in NLRP3 inflammasome activation. Nature **469:** 221–225.